Theoretical Modeling of Intra- and Inter-molecular Charge Transport

Lili Lin

To Zhongjie, Jiaxing and my parents.

Abstract

This thesis focuses on theoretical study of charge transport properties in molecular systems. The understanding of the transport process and mechanism in molecular systems is essential for the design of new functional molecular materials and molecular electronic devices. The molecular junctions and organic molecular crystals have been used as the model systems to highlight the usefulness of theoretical modelling. A molecular junction is a system that consists of one or several molecules sandwiched between two electrodes. The charge transport in molecular junctions is a very complex process that is affected by the interaction between molecules and electrodes, the surroundings, as well as electron-electron (e-e) and electron-phonon (e-p) couplings. When the molecule-electrode coupling is strong, the transport process can be very quick. If the e-p coupling is weak, the inelastic tunneling has only negligible contributions to the total current and the elastic electron tunneling plays the dominant role. Furthermore, the hopping process becomes dominant in the case of strong e-p coupling, for which the geometric relaxation of the molecule needs to be considered. In this thesis, we have examined these three kinds of transport processes separately.

The first studied system is a molecular junction consisting of aromatically coupled bimolecules. Its elastic electron tunneling property is simulated using Green's functional theory at density functional theory level. The dependence of the conductance of bimolecular junctions on the vertical distances, horizontal distances and the tilt angles has been systematically studied. The inelastic electron tunneling spectra (IETS) of molecular junctions have been calculated for several systems that were experimentally measured with conflicting results and controversial assignments. Our calculations provide the reliable assignments for the experimental spectra and revealed unprecedented details about the molecular conformations within the junctions under different conditions. It demonstrates that a combined theoretical and experimental IETS study is capable of accurately determining the structure of a single molecule inside the junction. The hopping process is a dominant charge transfer process in organic molecular crystals. We have studied the charge transport ability of four kinds of n-type organic semiconductor materials to find out the related structure-to-property relationship. It is done by adopting the quantum charge transfer rate equation combined with the random walk approach.

Preface

The work presented in this thesis was carried out at the Department of Theoretical Chemistry and Biology, School of Biotechnology, Royal Institute of Technology, Stockholm, Sweden and College of Physics and Electronics, Shandong Normal University, Jinan, P.R. China.

List of papers included in the thesis

Paper I   <u>Lili Lin</u>, Xiuneng Song, Yi Luo and Chuankui Wang, *Formation and Electronic Transport Properties of Bimolecular Junctions Based on Aromatic Coupling*, J. Phys.: Condens. Matter, 22 (2010) 325102-325107.

Paper II   <u>Lili Lin</u>, Chuankui Wang and Yi Luo, *Inelastic Electron Tunneling Spectroscopy of Gold-Benzenedithiol-Gold Junctions: Accurate Determination of Molecular Conformation*, ACS Nano, 5 (2011) 2257-2263.

Paper III   <u>Lili Lin</u>, Bin Zou, Chuankui Wang and Yi Luo, *Assignments of Inelastic Electron Tunneling Spectra of Semifluorinated Alkanethiol Molecular Junctions*, J. Phys. Chem. C, 115 (2011) 20301-20306.

Paper IV   <u>Lili Lin</u>, Xiuneng Song, Jiancai Leng, Zongliang Li, Yi Luo and Chuankui Wang, *Determination of the Configuration of a Single Molecule Junction by Inelastic Electron Tunneling Spectroscopy*, J. Phys. Chem. C, 114 (2010) 5199-5202.

Paper V   <u>Lili Lin</u>, Hua Geng, Zhigang Shuai and Yi Luo, *Charge Transport in Perylene Diimides Based n-type Organic Semiconductors*, submitted to Organic Electronics.

List of papers not included in the thesis

Paper I   <u>Lili Lin</u>, Jiancai Leng, Xiuneng Song, Zongliang Li, Yi Luo and Chuankui Wang, *Effect of Aromatic Coupling on Electronic Transport in Bimolecular Junctions*, J. Phys. Chem. C, 113 (2009) 14474-14477.

Paper II   Jiancai Leng, **<u>Lili Lin</u>**, Xiuneng Song, Zongliang Li, Yi Luo and Chuankui Wang, *Orientation of Decanethiol Molecules in Self-Assembled Monolayers Determined by Inelastic Electron Tunneling Spectroscopy*, J. Phys. Chem. C, 113 (2009) 18353-18357.

Paper III   Chuankui Wang, Bin Zou, Xiuneng Song, Yingde Li, Zongliang Li, **<u>Lili Lin</u>**, *Simulations of Inelastic Electron Tunneling Spectroscopy of Semifluorinated Hexadecanethiol Junctions*, Front. Phys. China, 4 (2009) 415-419.

Comments on my contribution to the papers included

I was responsible for the calculation and writing of papers I-V.

Acknowledgments

CONTENTS

Introduction

Charge transport as a fundamental phenomenon of electricity or electronics has long been the research focus. In 1729, Stephen Gray, the English physics, found that there are conductors and insulators. Since then, the human knowledge on electricity becomes gradually complete and profound. One of the commonly accepted facts is that the organic materials are insulators. That is, charges can not transport in organic materials. It is true in the macro world. When it goes to the micro world, like in one organic molecule, is this judgement still tenable? The answer definitely is "NO". In the 1950s, Westinghouse organized one conference named "Molecular Electronics" and devoted to the realization of the idea proposed by Arthur von Hippel that one can make electronic devices from atoms or molecules. However, they realized that it was really difficult and gave it up. Until 1974, Aviram and Ratner found theoretically the rectification of the current in a $D - \pi - A$ system and stated that molecules with specific design can realize specific functions.[1] Nevertheless, there was no experiment could prove their theoretical prediction until 1997, when Reed and coworkers performed the first measurement of the transport properties of a single molecular junction.[2]

From the 1980s, with the invention of Scanning Tunneling Microscopy (STM) and the progress in molecular self-assembly techniques, investigations on molecular junctions become increasingly prosperous. Lots of preparation techniques and detection methods on molecular junctions have been designed, such as the Mechanical Controllable Break Junction (MCBJ) method,[2–11] Scattering Tunneling Microscopy[12–14] and other methods combining these two techniques.[13,15–24] Correspondingly, measurement methods such as I(s),[25] and I(t) methods[26] have also been designed.

Theoretical understanding of transport mechanisms in molecular junctions started from the simulation of the STM image. Tersoff and Hamann stated that

the tunneling current in the STM measurement is proportional to the local density of states at the tip.[27] In 1994, Mujica and Ratner developed one simple model to calculate the conductance based on the elastic scattering Green's function theory and applied it to STM.[28,29] Quantum chemistry methods such as the semiempirical,[30–34] *ab initial*[35] and the density functional theory (DFT)[36–40] methods have also been developed to describe the transport process in molecular junctions. The most popular approach is the non-equilibrium Green's function (NEGF) method which describes the open system in a non-equilibrium situation with the DFT method.[41–43] Our group also developed one simple and intuitive first-principles approach[44,45] to study the charge transport properties in molecular junctions which is based on the elastic scattering Green's function theory, similar to what was proposed by Mujica and Ratner.[28,29]

All the above mentioned theories have been developed to deal with the elastic tunneling process, in which the charge transport from one electrode to the other obeys the energy conservation rule. However, the actual transport process in the molecular junctions is much more complex (see Fig. 1.1). Troisi and Ratner classified the transport regimes based on some important energy parameters.[46] One of the parameters is the injection energy gap (ΔE) that is defined as the energy difference between the Fermi level and the orbital closest to it, for instance, the highest occupied molecular orbital (HOMO) or the lowest unoccupied molecular orbital (LUMO). Another one is the spectra density or energy broadening (Γ) resulted from the coupling between the molecule and the electrodes. When both ΔE and Γ are large, the Laudauer regime dominates the transport process. If Γ is small, higher energy is needed for electrons to overcome the barrier and the electron tunneling will be the main mechanism. Both transport regimes are far from resonance and belong to the elastic tunneling. At both regimes, the electron-phonon (e-p) coupling is relatively weak ($\frac{M}{\sqrt{(\Delta E)^2+\Gamma^2}} \ll 1$, where M is the e-p coupling), and the vibration signals are reflected as the regular inelastic electron tunneling spectroscopy (IETS). When ΔE is close to zero, the transport electrons will be resonant with the electronic energy level of the molecule. If Γ is not too large, the electron can stay at the molecule transiently to deform the molecule (polaronic form). Resonant IETS (RIETS) may present as the sidebands in the conductance-voltage plot, and it reflects the vibration signals of intermediate molecular ions. When the e-p coupling is strong, electron hopping from the molecule to electrodes or between molecular sites will become the main transport process. When both ΔE and Γ are small enough, coulomb blockade phenomenon induced by e-e interaction will appear, which is not in our consideration here. The detailed classification of these transport regimes can be found in the review papers.[46,47] In this thesis, only three kinds of regimes, that is, coherent tunneling, normal IETS and hopping are

investigated.
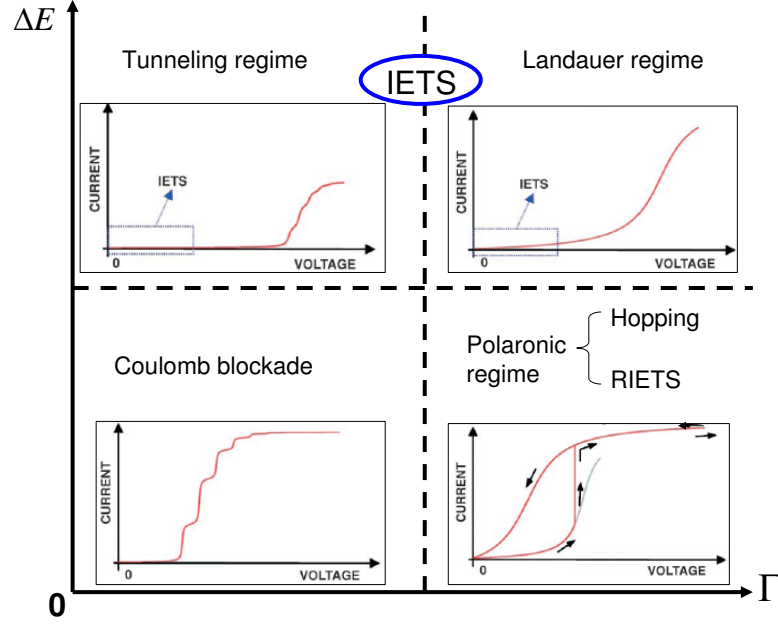
Figure 1.1: *Classification of transport regimes according to the injection energy gap, the broadening factor and the e-p coupling.[46]*

The IETS signals were first detected in the metal-metal oxide-metal tunneling junctions by Jaklevic and Lambe[48] in 1966. When they performed measurement on the derivative $\partial G/\partial V$, they found vibration signals of the adsorbate molecules in the junction. They believed that transport electrons with energy large enough ($eV \geq \hbar\omega$) can exchange energy with the molecule in the junction. Although the IETS technique was established very early, the complicated setup and the difficulty in interpretation of the spectra make it hard to be applied widely. The first IETS experiment on molecules was performed by Wilson Ho and co-workers[49] in 1998. With the improvement on techniques, IETS gradually becomes popular as an important detection technique to obtain the vibration and structure information in molecular junctions. Many theoretical methods have been developed to interpret the inelastic process, and most of them were derived from the scattering theory or NEGF theory.[50–59] We also generalized our elastic scattering Green's function theory by including the e-p coupling and successfully applied it to many systems.[60–63]

So far, the electron tunneling process is assumed to be too quick to influence the geometry of the molecule and the molecule can stay in the ground state. When the e-p coupling is strong and the charges stay at the molecule for a long-enough

time to induce geometric change of the molecule before they run away, another process called as hopping appears. It always happens in junctions with long molecules and at high temperatures. To describe this process, master equation methods have been developed and successfully applied to the transport in DNA.[64–68] Hopping process in molecular junctions was less studied than the coherent tunneling process since most experiments were performed on small molecular systems. Recently, more and more experiments found that the transport mechanism can shift from the tunneling to the hopping in molecular junctions with the elongation of the molecules.[69–72] Theoretical simulations of the hopping process in molecular junctions should be paid more attention. Up to now, most theoretical simulations of hopping process only stay at the charge transfer rate calculation which can not be directly compared with the experimental results (conductance values),[71,72] although the approximate relationship between the conductance and the charge transfer rate has been established by Nitzan and Ratner.[73,74] As we know, the hopping process is also the main transport mechanism in organic molecular materials. Here we studied the charge hopping process in organic molecular materials by adopting the quantum charge transfer rate equation combined with the random walk approach developed by Shuai's group.[75]

In this thesis, we focus on charge transport phenomena that involve three different kinds of transport regimes in molecular systems. In Chapter 2, we will first introduce our first-principles approach based on the elastic scattering Green's function theory for the study of elastic transport in molecular junctions. Based on our method, the aromatic effect on the elastic electron transport properties of bimolecular junctions will be presented. In Chapter 3, the inelastic electron tunneling mechanism and the physical qualities to characterize it will be introduced first. The significance to study IETS and its peculiar propensity rules will also be presented. Following that, our generalized inelastic electron tunneling theory by adding the e-p coupling into our elastic electron tunneling theory will be shown. At last, the influence of the electrode topography, electrode distances, molecular rotation angles and the tilt angles on the IET spectra will be presented. In Chapter 4, the study on the charge transfer in organic molecular materials will be presented. Based on the hopping model, the quantum charge transfer rate equation deduced from Fermi Golden Rule will be given. Following that, the calculation methods of parameters involved in the rate equation and the charge mobility will be summarized. A summary of the included papers will be shown in Chapter 5.

Elastic Transport in Molecular Junctions

When electrons transport through a metal-molecule(s)-mental junction, they may interact with the molecule(s). If the interaction is very weak, the probability for electrons to exchange energy with the molecule(s) is small, and the inelastic tunneling process can be ignored. For theoretical simulations, it is always convenient to start from the simplest situation based on reasonable approximations. To investigate the charge transport in molecular junctions, the elastic transport process is always chosen as the starting point where the electrons transport through the junction with energy conservation. For small molecules sandwiched between two metal electrodes, the main transport mechanism is proven as the coherent tunneling process which shows that the conductance decreases exponentially with the increase of molecular lengths. Besides the length dependence of the conductance, there are also many other factors that can influence it, such as electrode materials,[19,40,76–79] molecular conformations,[80–82] substitutions on the molecule,[83–87] anchor groups[88–94] and contact configurations.[26,95–98] The solvent,[2,23,97,99–104] temperatures[91,97,103–111] and the load[112,113] coming from the tip can also influence the transport properties of molecular junctions. All these factors have been widely studied both in experiments and theory to some extent. For self-assembly monolayer, the molecules around the target molecule can also present significant influence. Some theoretical works have been devoted to the intermolecular interaction on charge transport properties in bimolecular junctions.[114–118]

As mentioned in Chapter 1, many theoretical approaches have been developed to describe the elastic tunneling process in molecular junctions. Here we will simply introduce the method developed by our group, which is based on the elastic scattering Green's function theory and adopts first-principles methods. In the second section, one application based on our method will also be presented where the aromatic coupling effect on the electron transport properties of bimolecular

junctions is investigated.

2.1 Elastic transport theory

The method to investigate the elastic charge transport properties is based on the work of Mujica, Kemp and Ratner[29]. The model system is composed of three subsystems: the source electrode (S), the central molecule (M) and the drain electrode (D) (see Fig. 2.1). Because the localized atomic orbitals are adopted as the basis sets in our first-principles calculation, the Hamiltonian of the system can be written in a contracted pattern:

$$H = H_S + H_M + H_D + U \tag{2.1}$$

where H_S, H_M and H_D are the Hamiltonian of the source electrode, the molecule and the drain electrode respectively. U represents the interactions between subsystems and can be written as follows if only the interaction between neighboring subsystems is considered:

$$U = H_{SM} + H_{MS} + H_{MD} + H_{DM} \tag{2.2}$$

where H_{SM} or H_{DM} is the interaction between the source or drain electrode and the molecule. Correspondingly, the eigen wavefunctions (molecular orbitals) for this system can also be expressed as:

$$\psi = \psi_S + \psi_M + \psi_D \tag{2.3}$$

Figure 2.1: *Model system of a molecular junction in our theoretical method.*

Based on the generalized Kubo formula for the stationary carrier conductance[119] and adopting the three-dimension electrode model,[45] the current density can be calculated as:

$$
j_{DS}^{\alpha(\beta)} = \frac{2emK_BT}{\hbar^3} \int_{eV}^{\infty} dE_Z \left\{ ln[1 + \exp(\frac{E_f - E_Z + eV}{K_BT})] - ln[1 + \exp(\frac{E_f - E_Z}{K_BT})] \right\}
$$
$$
\times |T^{\alpha(\beta)}(E_Z)|^2 r_{3s}^2 \rho_{1d}^{S\alpha(\beta)} \rho_{1d}^{D\alpha(\beta)}
\tag{2.4}
$$

where e and m are the charge and mass of one electron respectively, K_B is the Boltzmann constant and T is the temperature at which electrons transport through the junction. A distinction should be made between T (temperature) and the transition function $T^{\alpha(\beta)}(E_Z)$. E_f and E_Z are the fermi energy of the electrode and the energy along the Z direction for the transport electron. Parameters α and β represent the up and down spin of electrons respectively. r_{3s} is the average radius of transport electrons and can be written as:

$$r_{3s} = \hbar(\frac{9\pi}{4})^{\frac{1}{3}}\frac{1}{\sqrt{2mE_f}} \tag{2.5}$$

The electronic density at the source (drain) electrode $\rho_{1d}^{S\alpha(\beta)}$ ($\rho_{1d}^{D\alpha(\beta)}$) is calculated as:

$$\rho_{1d}^{\alpha(\beta)} = \frac{1}{2\pi\hbar}\sqrt{\frac{2m}{E_Z}} \tag{2.6}$$

In the equation for current density (Eq. 2.4), the transition function $T^{\alpha(\beta)}(E_z)$ is the most important parameter. Now we will introduce the calculation of $T^{\alpha(\beta)}(E_z)$.

Based on the elastic scattering Green's function theory,[120] the transition function can be written as:

$$T(E) = U + UG(E)U \tag{2.7}$$

where U, the scattering potential, is the interaction between subsystems here and $G(E)$ is the Green's function:

$$G(E) = \frac{1}{E - H} \tag{2.8}$$

The transition from the initial state $\sum_i |S_i\rangle$ to the final state $\sum_j |D_j\rangle$ can be calculated as:

$$\begin{aligned}
T_{DS}(E) &= \sum_{i,j}\langle D_j|U + UG(E)U|S_i\rangle \\
&= \sum_{i,j}\langle D_j|U|S_i\rangle + \langle D_j|UG(E)U|S_i\rangle
\end{aligned} \tag{2.9}$$

where the interaction between the source and the drain can be ignored since it is normally very weak. The transition function can be expressed with the atomic sites as:

$$\begin{aligned}
T_{DS}(E) &= \sum_{k',k,n}\frac{\sum_j\langle D_j|U|k'\rangle\langle k'|n\rangle\langle n|k\rangle\sum_i\langle k|U|S_i\rangle}{E - E_n + i\Gamma_n} \\
&= \sum_{k',k,n}V_{Dk'}V_{Sk}g_{k',k}^n
\end{aligned} \tag{2.10}$$

7

where k and k' are atomic sites on the bare molecule, n is the label of molecular orbitals for the extended molecule and D_j (S_i) is the atomic site on the drain (source) electrode. $V_{Dk'}$ (or V_{Sk}) is the coupling energy between the drain electrode (or source electrode) and atomic site k' (or k), they can be calculated according to:

$$V_{Dk'} = \sum_j^D \sum_m^{k'} \sum_n^{OCC} C_{jn} C_{mn} \langle \phi_j | U | \phi_m \rangle$$

$$V_{Sk} = \sum_i^S \sum_m^k \sum_n^{OCC} C_{in} C_{mn} \langle \phi_i | U | \phi_m \rangle$$

(2.11)

where ϕ is the atomic orbital and C_{jn} (C_{mn}, C_{in}) is the molecular orbital coefficient. The Green's function can be written as:

$$g_{k',k}^n = \frac{\langle k' | n \rangle \langle n | k \rangle}{E - E_n + i\Gamma_n}$$

(2.12)

where Γ_n is the broadening factor and it can be calculated according to:

$$\Gamma_n = \pi V_{Sk}^2 \sum_i^k |\langle n | \phi_i \rangle|^2 n^S(E) + \pi V_{Dk'}^2 \sum_j^{k'} |\langle n | \phi_j \rangle|^2 n^D(E)$$

(2.13)

where $n^S(E)$ and $n^D(E)$ are the density of states for the source and drain electrodes respectively.

From the current density calculated as above, the current can be obtained by multiplying the injection area:

$$I = \pi r_{3s}^2 j_{DS}$$

(2.14)

and the conductance can be calculated as the derivative of the current:

$$G = \frac{\partial I}{\partial V}$$

(2.15)

In our calculation, the cluster model where the molecule connected with several metal atoms is adopted. The rest part of the electrode is described by the effective mass approximation. This approximation has been proved to be reasonable because the electrons are mostly localized on the molecule and the first layer of the electrode. Based on this model, different contact configurations can be simulated and the coupling energy between the molecule and the electrodes can be calculated, which is very intuitive for us to understand the interaction between the molecule and the electrode. The method based on the elastic scattering Green's

function theory mentioned above has been implemented in the code QCME (Quantum Chemistry for Molecular Electronics).[121] The calculation procedures have been shown in Jiang' PhD thesis.[122] This package can be interfaced with any quantum chemistry program, and here we always based on the quantum chemistry calculation from `Gaussian 03` program.[123] Many systems including large and small with conjugated and saturated molecules have been investigated based on our method, and good agreement with the experimental counterparts have been generally obtained.[44,45,124] Attention should be paid that the effect of the bias on the geometric and electronic structures of molecular junctions is neglected here, consequently our method is only applicable in the low bias. This is the drawback of our method in comparison with that of non-equilibrium Green's function (NEGF) theory. Many programs based on NEGF theory have been developed in recent years, such as Atomistix ToolKit (ATK),[41–43] TranSIESTA,[41,42] McDCal,[43] Smeagol[125,126] and others.

2.2 Aromatic coupling effect

The study of intermolecular interactions comes from the investigation on the charge transport in self-assembled monolayers (SAM). In dense SAM, the charge transfer among neighboring molecules is possible. Early in 1998, Yaliraki and Ratner have studied the charge transport properties of adlayers of molecules by considering transport through two identical wires using a model Hamiltonian.[127] They found that there is indirect interaction between two wires by mutual interaction with reservoirs. If there is direct intermolecular interaction, the conductance maximum appears when the transfer happens in the middle of the molecules rather than the ends, for the nonresonant case. At the resonant situations, the conductance values oscillate with the variation of the transfer positions. In 2000, Lang and Avouris proposed that there are two kinds of interactions in parallel atomic wires: the direct interaction between two wires and the indirect interaction through electrodes.[128] Later, Emberly and Kirczenow also proposed one model for SAM where each molecule bonds with only one electrode.[114,117] They thought that the charges are transported by the overlapping of two molecules in the dense SAM and through one single molecule in the dilute SAM. Liu *et al.* performed first-principles study on the conductance of bimolecular junctions and found that the indirect coupling between two molecules is the main interaction.[115] Geng *et al.* also investigated the same systems but with imperfect contacts, and the indirect interaction is supposed to be ignored.[116] The negative differential resistance phenomenon has also been observed in the bimolecular junctions when the distance between two molecules is small enough.[118]

From the research mentioned above, one can find that the interaction between two molecules in a bimolecular junction is very important to the charge transport properties. There are both direct and indirect interactions between the two molecules. When both of the molecules are connected with two electrodes, both interactions may be involved. When each molecule only contacts with one electrode, the direct interaction could be the main interaction. All the above theoretical investigations are based on models or aromatic systems with $\pi - \pi$ interaction. There was no experimental proof of the formation of bimolecular junctions until 2008.
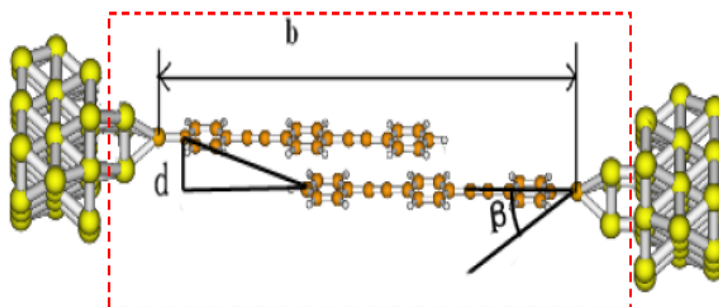
Figure 2.2: *Conformations of the bimolecular junction. The dashed frame contains the extended molecular system. Parameter b and d represent the lateral and vertical distance, β is the tilt angle of the lower molecule relative to the upper one.* **Adapted with the permission from The Journal of Physical Chemistry C, Copyright 2009, American Chemical Society.**

It is commonly accepted that the molecule with only one anchor group can not connect with two electrodes very well, or to say, molecular junctions can not form. In 2008, Wu and co-workers found that there are significant statistic conductance peaks for the Oligo (phenylene ethynylene) (OPE) molecules with only one anchoring group in the junction prepared with the Scattering Tunneling Microscopy Break Junction (STM-BJ) method.[129] It is suggested that there should be two molecules sandwiched between two electrodes by the aromatic coupling with each molecule contacted with only one electrode through the sulfur atom. Aromatic coupling is one kind of special weak interaction between molecules with aromaticity. The interaction between π electrons will make the molecules form specific stacking configurations. Following Wu's work, we investigated the aromatic effect on the charge transport properties of bimolecular junctions theoretically. The model of a typical bimolecular junction is shown in Fig. 2.2. Two molecules connect with the each electrode through the end sulfur atom and parallel with each

other. Parameter b and d represent the lateral and vertical distances between two molecules. β is the tilt angle of the lower molecule relative to the upper molecule. Here, the conformation with b=2.88 nm and $\beta = 0$ is adopted.

2.2.1 Vertical distance dependence

The conductance-voltage characteristics of the bimolecular junctions with different vertical distances are shown in Fig. 2.3. The first conductance plateaus for the four conformations appear at the same voltage (about 0.8 V), while the conductance values at the plateaus are totally different. With the decrease of the vertical distance d, the conductance value gets larger.

Figure 2.3: *Conductance curve of bimolecular junctions with vertical distance 0.28 nm, 0.31 nm, 0.33nm and 0.36nm.* **Reproduced with the permission from The Journal of Physical Chemistry C, Copyright 2009, American Chemical Society.**

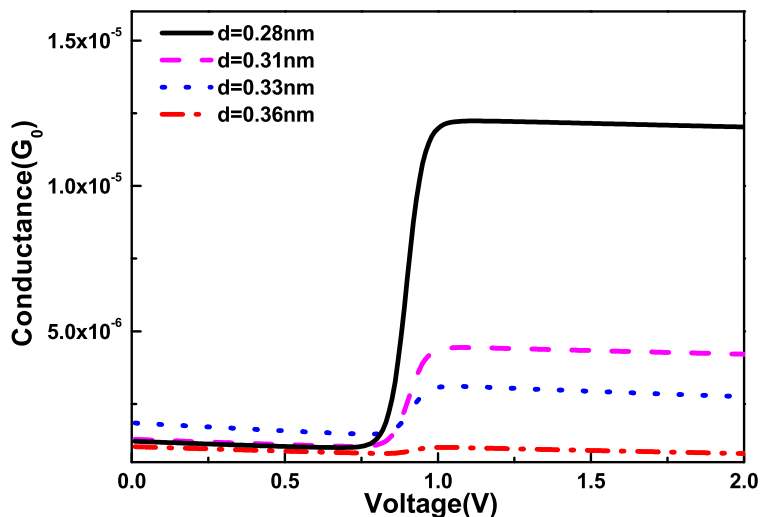The charge distributions of the HOMO and LUMO+2 that have significant contribution to the conductance plateau are shown in Fig. 2.4. It is shown that the overlap of the HOMO is much larger than that of the LUMO+2, which also indicates the strong interaction between the two molecules. For the LUMO+2, the overlap gets stronger with the decreasing of the vertical distance, which is

consistent with that of the HOMO. When the vertical distance is 0.36 nm, the
overlap is so small that the interaction becomes very weak.
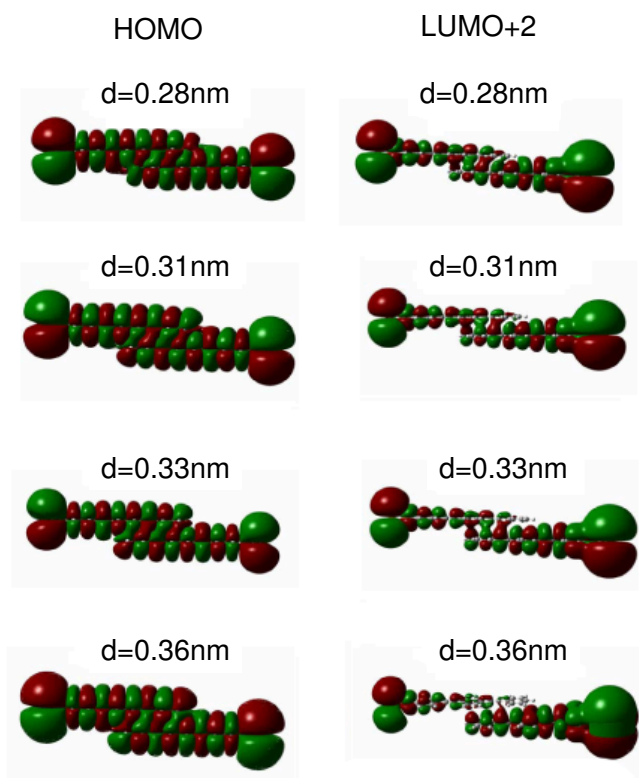
Figure 2.4: *Charge distributions of HOMO and LUMO+2 for the bimolecular junctions with different vertical distances.* ***Reproduced with the permission from The Journal of Physical Chemistry C, Copyright 2009, American Chemical Society.***

It is commonly accepted that there are two possible transport pathways in
bimolecular junctions. One is that electrons tunnel from one electrode to the
other directly. The other pathway is that electrons transport to one molecule, then
jump to the other molecule and subsequently tunnel to the other electrode. When
both ends of the two molecules are connected with both two electrodes, the first
tunneling path may dominate the transport process. However, when only one end
of each molecule contact with each electrode, the second path is definitely the only
effective channel. The coupling between the two molecules in the junctions thus
determines the transport properties. The coupling energy between two molecules

can be calculated according to

$$V_{MM'} = \sum_{k}^{M} \sum_{k'}^{M'} \sum_{n}^{OCC} C_{kn} C_{k'n} \langle \phi_k | U | \phi_{k'} \rangle \qquad (2.16)$$

where M and M' represent the two molecules respectively. ϕ_k and $\phi_{k'}$ are the atomic orbitals of two molecules. C_{kn} and $C_{k'n}$ are molecular orbital coefficients. The calculated coupling energies between two molecules are 7.95 eV, 2.78 eV, 1.34 eV and 0.39 eV, when the vertical distances are 0.28 nm, 0.31 nm, 0.33 nm, and 0.36 nm, respectively. The coupling energy drastically decreases with the increase of the vertical distance. It can be seen that when the vertical distance goes beyond 0.36 nm, the coupling energy becomes very small and the formation of bimolecular junction gets very difficult.

2.2.2 Tilt angle dependence

Figure 2.5: *Conductance values of bimolecular junctions calculated at 1.0 V bias with different tilt angles.* **Reproduced with the permission from The Journal of Physical Chemistry C, Copyright 2009, American Chemical Society.**
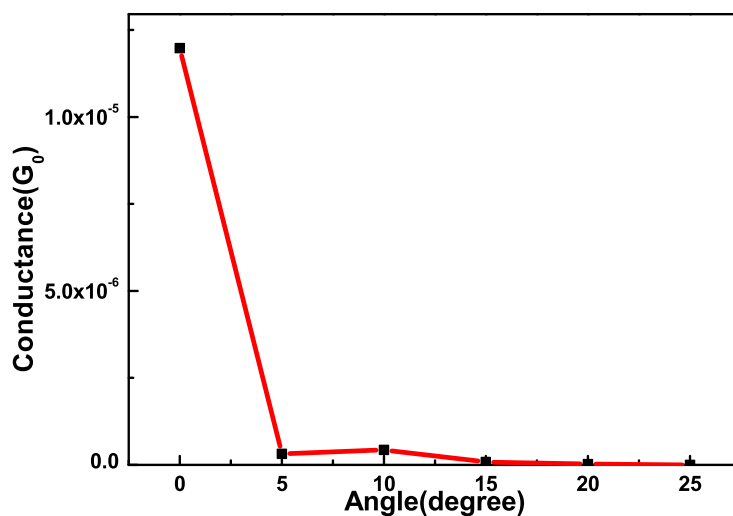
When the vertical distance and horizontal distance are both fixed, one molecule may also tilt with respect to the other. Here the configuration with b=2.88 nm

and d=0.28 nm has been adopted. When the tilt angle changes, the conductance calculated at 1.0 V bias is shown in Fig. 2.5. The conductance is very sensitive to the tilt angle. When the tilt angle is only 5 degree, the conductance decreases to $3.1 \times 10^{-7} G_0$ from $1.2 \times 10^{-5} G_0$. When the tilt angle is larger than 5 degree, the conductance is so small that it will be difficult to detect the conductance. Our calculation also indicates that the coupling energy between the two molecules reduces to 0.076 eV when the tilt angle is 5 degree. Such a small coupling energy makes it very difficult for electrons to transport from one molecule to the other, and results in very small conductance. Our calculation indicates that the conductance of bimolecular junctions should be detectable on the almost parallel configurations rather than the ones with tilt angles.

2.2.3   Dependence of horizontal distances
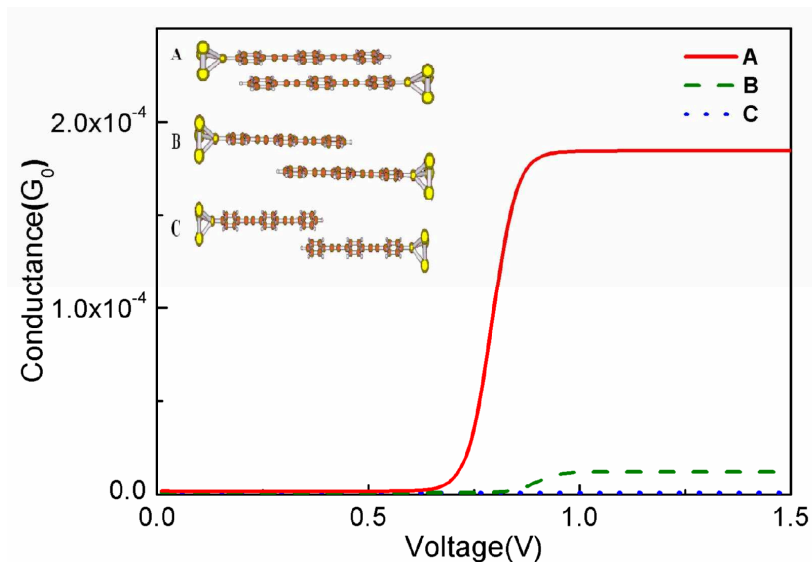
Figure 2.6: *Conductance curves of bimolecular junctions with different horizontal distances. The conformations of A, B and C are shown in the insert.* **Reproduced with the permission from The Journal of Physical Chemistry C , Copyright 2009, American Chemical Society.**

When the vertical distance is fixed as 0.28 nm and the tilt angle β is zero, the other stacking configurations with horizontal distances change are shown in the insert of Fig. 2.6. The conformations A (b=2.18 nm), B (b=2.88 nm) and C (b=3.57 nm) have different overlapping benzene rings. The calculated coupling energies for A, B and C are 12.74 eV, 7.95 eV and 3.33 eV, respectively. The ratio is approximated

14

as 3:2:1, which is also consistent with the number of overlapping benzene rings. The calculated conductance curve indicated that the conductance value at the plateaus decreases as the horizontal distance increases. One of the reasons is the enlarged electrode distances, the other is the reduction of the overlapping. It can also be found that the first conductance plateau shows up at different voltages. The first conductance plateau arises at lower voltage for the conformation A than B, while no significant conductance plateau appears in the interested bias for the conformation C.

In conclusion, the aromatic coupling is found to be the key for the formation of bimolecular junctions. In addition, it strongly depends on the conformations of the bimolecular junctions and can significantly influence the transport properties. Our calculations indicate that the increase of both vertical (d) and horizontal (b) distances can reduce the coupling energy between two molecules and the conductance values. Besides, the conductance drastically reduce to very small value when both molecules are mutually tilted. This fact could be used to argue that a good bimolecular junction adopts the parallel stacking configuration.
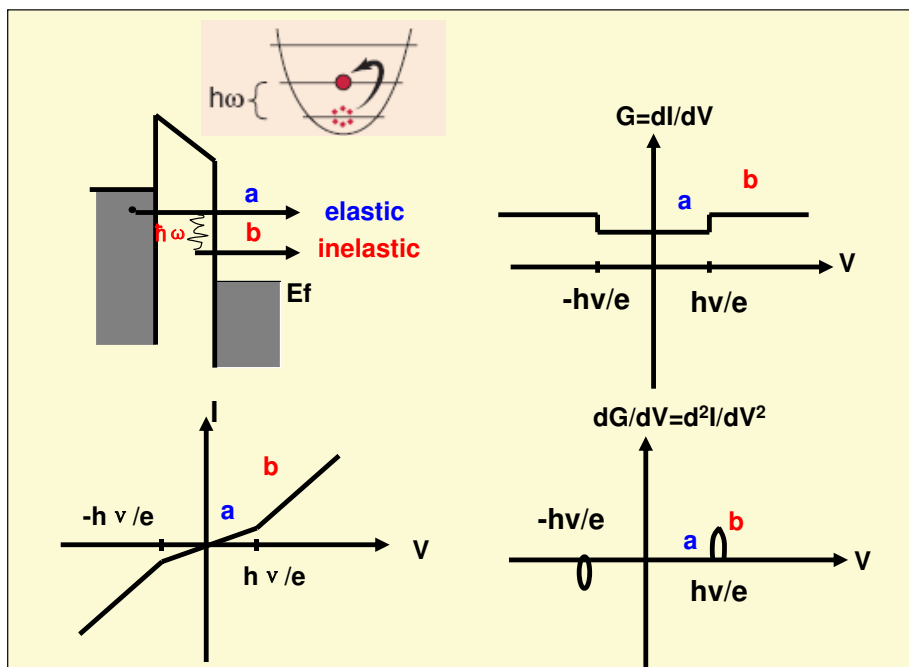
Inelastic Electron Tunneling Spectroscopy

The elastic electron tunneling process has been introduced in Chapter 2. In this chapter, the inelastic electron tunneling process, in which the energy exchange takes place between the electron and the molecule, will be discussed. It should be noted that the interaction between electrons and molecular vibrations, *i.e.* a kind of electron-phonon (e-p) interaction, is assumed to be still very weak, and the electron state is far away from the resonance. The outline of this chapter is as follows: first the inelastic mechanism of the inelastic electron tunneling will be presented, with three basic physical qualities to describe the inelastic electron tunneling spectroscopy (IETS); then the significance of IETS will be discussed as a powerful tool especially to characterize the conformations of molecular junctions; the propensity rules of IETS will be reviewed; the vibration modes for two kinds of typical groups will also be shown; and finally, our own approach for inelastic electron transport will be introduced and applied to establish the spectra-conformation relationship.

3.1 Transport mechanism of IETS

In Fig. 3.1, the transport mechanism of IETS is schematically shown. A molecule with discrete states is located between two electrodes (the grey parts) whose energy levels are continuous. After a small bias voltage is applied, the electrons in the left electrode can tunnel through the molecule to the right one elastically ("a" process), or inelastically ("b" process) if the bias voltage happens to be equal to the energy difference of the molecular vibrational level ($\hbar\omega$). In the inelastic process, the energy of the inelastic electron could transfer to the molecule to induce vibrational excitations. A new channel for the electron to transport is thus opened, which is reflected as an abrupt increase in the current curve, a step in the conductance plot and a peak in the IET spectrum. However, it is worth noting that since

the probability of inelastic electron tunneling is very low compared to that of the elastic process, the contribution from inelastic electrons to the total current is quite small.

Figure 3.1: *Inelastic electron tunneling mechanism: "a" is the elastic process; "b" represents the inelastic process.*[130]

According to the mechanism of IETS, it can be seen that the positions where peaks appear correspond to the frequencies of molecular vibration modes. It mainly depends on the molecule itself, although the coupling between the molecule and the electrodes is also important. The peak intensity of the IET spectrum greatly depends on the e-p coupling within the molecular junction, which is usually the most difficult part for theoretical simulations. The electrode distance, the contact configuration and the conformation of the molecule within the junction have been found to have significant influence on the relative intensity of the IET spectrum[60,61,131,132]. As a result, theoretical simulations combined with experiments can be adopted to determine the detailed structural information of the molecular junction. In addition to the position and intensity of peaks in the IET spectrum, the line width of the peak is also an important parameter. Apart from the intrinsic broadening, which is induced by the lifetime of the vibrational state, there are two other broadening factors, the modulation and thermotic broadenings, that

can influence the line width of the peak. The modulation broadening is resulted from the detection of the second-order harmonic signals in the IETS measurement technique. To reduce the line width, the IETS is often performed at low temperatures (like 4.2 K). The modulation broadening of the vibration peak in the IET spectrum was stated as $1.2V_m$, where V_m is the modulation voltage[133]. The typical thermotic broadening was also proposed as $5.4K_BT/e$[133]. The lineshape of the intrinsic broadening has a Lorentz line profile which assumes:

$$I(\omega) = \frac{\Gamma}{2\pi[(\omega - \omega_{fi})^2 + \Gamma^2]} \tag{3.1}$$

where $I(\omega)$ is the intensity of the vibration peak, ω_{fi} is the vibration energy difference between two vibration levels, and Γ is the broadening factor. In our theoretical simulations, the Lorentz lineshape is adopted to compare with the experimental results.

3.2 Significance to study IETS

IETS is a unique spectral tool that can reflect molecular vibration characteristics. It has become the primary technique to probe the details in nanoscale devices. The IETS has many advantages for applications, which makes it very popular.

1. High sensitivity

Unlike the Raman and Infrared spectra which are detected in the samples with more than thousands of molecules, IETS signals can be detected for only one or several molecules. It is more sensitive than the optical spectroscopic techniques.

2. Wide spectra range

The energy of IET spectra ranges from $50 \sim 500meV$ ($400 \sim 4000cm^{-1}$), which covers almost all the vibration modes of the molecules. In addition, it also corresponds to the spectra region of Infrared spectrometer, and its results can be verified by comparing with the infrared spectra.

3. No selection rules

IET spectrum is induced by the interaction between tunneling electron and the molecule. It is different from other optical spectra such as Raman and Infrared spectra in which only a part of vibration modes can be detected. There are no section rules for the IETS. As a result, some transitions forbidden in optical spectra can be active in the IET spectrum. It can complete the investigation of vibration modes of molecules.

Based on the particular characteristics of IETS, it has been widely used to detect the details within molecular junctions. It not only can confirm the existence of molecules in the junction, but also tell the conformation variations in the junction. A combination of theoretical modeling and experimental measurements can firmly establish the conformation-spectrum relationship, which can help us to understand better about the electron transport in molecular devices.

3.3 Propensity rules of IETS
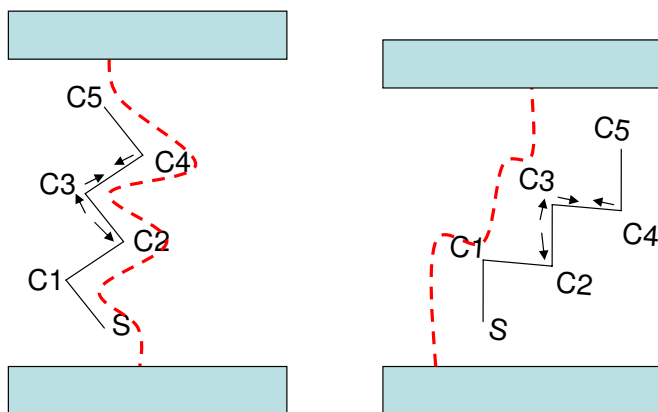
Figure 3.2: *Schematic diagram of electron tunneling paths. The molecule is perpendicular (left) or tilt (right) relative to the electrode. The arrows indicate the vibration orientation and the dash lines represent the tunneling paths.*[134]

Although there is no selection rules for IETS, some propensity rules have been proposed by several groups. Early in 1976, Kirtler and co-workers have proposed that symmetric vibration modes with oscillating dipole moment perpendicular to the electrode surface have larger intensity than those asymmetric modes with oscillating dipole moment parallel to the surface[135]. Lorente and Persson proposed a symmetry selection rule which is based on the symmetry of the vibration modes, the intermediate state and the projected density of states on orbitals of bare molecule[52]. Troisi and Ratner proposed a propensity rule for IETS both based on symmetry and pathways[136]. In addition, they also indicated that the quasi-symmetric vibration modes can also be active in the IETS by the new tunneling path[134], as shown in Fig. 3.2). The C2-C3 and C3-C4 stretching vibrations are considered as the quasi-antisymmetric vibration modes. According to the symmetry rules proposed earlier, the antisymmetric vibration modes should not be

active in the IETS if the antisymmetric vibration atoms are in the main tunneling path. However, when the molecule tilts relative to the electrode surface, the new tunneling path electrode-C3-C2-C1-S-electrode can open and compete with the original path electrode-C5-C4-C3-C2-C1-S-electrode. In this new tunneling path, the quasi-antisymmetric vibration mode can contribute to the IETS. Our recent works have also confirmed the propensity rules proposed by Troisi[134] and Kirtler[135]. It is noted that in 2008, Paulsson reported the unified description of inelastic propensity rules[137], which summarized all previous known rules.

3.4   Molecular vibration modes

Up to now, the IETS of different aromatic and saturated molecules have been intensively studied. There are 3N-6 (3N-5) vibration normal modes for a molecule, where N is the number of the atoms in the molecule. Generally, the vibrations of a molecule include the stretching (along the direction of the chemical bond) and bending (perpendicular to the bond direction) patterns. For convenience, the vibration modes of two basic groups will be presented. The atomic motion in vibration modes related to the CH_2 group is shown in Fig. 3.3. The name, label and frequencies of these vibration modes are listed in Table. 3.1. The labeling of these vibration modes is based on the calculation of C_3H_8 molecule using B3LYP functional and 6-31G* basis set in `Gaussian 03` program.
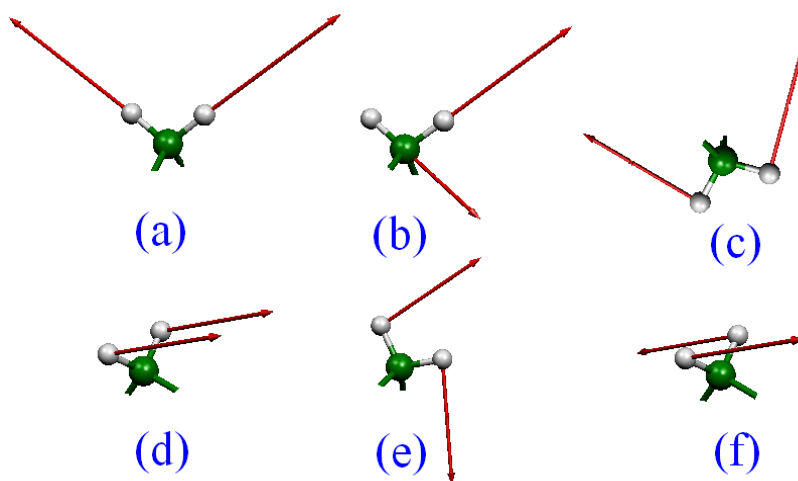
Figure 3.3: *Vibration pictures for the vibration modes of CH_2 group.*

Table 3.1: *The name, label and frequencies of vibration modes of CH_2 group*

	Name	Label	Frequency (cm^{-1})
(a)	symmetric stretching	$\nu_s(CH_2)$	3033
(b)	anti-symmetric stretching	$\nu_a(CH_2)$	3058
(c)	symmetric scissoring	$\delta_s(CH_2)$	1544
(d)	wagging	$w(CH_2)$ or $\gamma_w(CH_2)$	1387
(e)	rocking	$\rho(CH_2)$ or $\delta_r(CH_2)$	759
(f)	twisting	$t(CH_2)$ or $\gamma_t(CH_2)$	1332

The benzene molecule is the basic building block of aromatic molecules. The presentation of its vibration modes is very important for us to sign the IET spectra. There are 30 vibration modes for a benzene molecule. Based on the Wilson-Varsanyi label method, the vibration modes are classified and signed. According to its vibration characteristics, the 30 vibration modes can be classified into nine groups. The detail classifications can be seen in the **Appendix**.

3.5   Theoretical method

Based on the elastic transport theory mentioned above, the vibration effect can be uniformly treated. In this case, the Hamiltonian of the system can be written as the sum of electronic Hamiltonian and the vibration counterpart. Based on the Born-Oppenheimer approximation, the vibration coordinates can be written as the parameter of the electronic Hamiltonian.

$$H = H(Q,e) + H(Q) \tag{3.2}$$

where $H(Q,e)$ and $H(Q)$ are the electronic and vibration Hamiltonian respectively. Correspondingly, the wavefunction for the system can be written as:

$$\psi = \psi(Q,e)\Theta(Q) \tag{3.3}$$

where $\psi(Q,e)$ and $\Theta(Q)$ are electronic and vibration wavefunctions. Based on the harmonic approximation, the electronic wavefunction can be expanded and truncated to the second term:

$$\psi(Q,e) = \psi(Q_0,e) + \frac{\partial \psi(Q,e)}{\partial Q}\Big|_{Q=Q_0} \tag{3.4}$$

When the vibration effect is considered, the transition function $T(E)$ can be written as:

$$T(E) = \sum_{k'}\sum_{k}\sum_{n} V_{Dk'}V_{Sk}\sum_{\nu'\mu\nu} g_{k',k}^{n,\nu',\mu,\nu} \tag{3.5}$$

where $V_{Dk'}$ and V_{Sk} are coupling energy. They do not depend on the vibration coordinates and are equal to the coupling energy in the elastic theory. Here $g_{k',k}^{n,\nu',\mu,\nu}$ contains all the vibration information and can be calculated as:

$$g_{k',k}^{n,\nu',\mu,\nu} = \frac{\langle\Theta^{\nu'}(Q)|\langle k'(Q,e)|n(Q,e)\rangle|\Theta^{\mu}(Q)\rangle\langle\Theta^{\mu}(Q)|\langle n(Q,e)|k(Q,e)\rangle|\Theta^{\nu}(Q)\rangle}{E - E_n - \sum_a n_a\hbar\omega_a + i\Gamma_n}$$

(3.6)

where $\Theta^{\nu'}(Q)$, $\Theta^{\mu}(Q)$ and $\Theta^{\nu}(Q)$ are vibration wavefunctions. $k'(Q,e)$ and $k(Q,e)$ are electronic wavefunctions for atomic site k' and k respectively. $n(Q,e)$ is the eigen-wavefunction (molecular orbital) for the Hamiltonian. n_a is the vibration quantum number for vibration mode a. Based on the harmonic approximation, the first integral at the numerator of $g_{k',k}^{n,\nu',\mu,\nu}$ can be written as:

$$\langle\Theta^{\nu'}(Q)|\langle k'(Q,e)|n(Q,e)\rangle|\Theta^{\mu}(Q)\rangle$$
$$= \langle\Theta^{\nu'}(Q)|\langle(k'(Q_0,e) + \sum_{a'}\frac{\partial k'(Q,e)}{\partial Q_{a'}}|_{Q=Q_0}Q_{a'})|(n(Q_0,e) + \sum_{b}\frac{\partial n(Q,e)}{\partial Q_b}|_{Q=Q_0}Q_b)\rangle|\Theta^{\mu}(Q)\rangle$$
$$= \langle\Theta^{\nu'}(Q)|\Theta^{\mu}(Q)\rangle\langle k'(Q_0,e)|n(Q_0,e)\rangle$$
$$+ \langle\sum_{a'}\frac{\partial k'(Q,e)}{\partial Q_{a'}}|_{Q=Q_0}|\sum_{b}\frac{\partial n(Q,e)}{\partial Q_b}|_{Q=Q_0}\rangle\langle\Theta^{\nu'}(Q)|\Theta^{\mu}(Q)\rangle$$
$$+ \langle k'(Q_0,e)|\sum_{b}\frac{\partial n(Q,e)}{\partial Q_b}|_{Q=Q_0}\rangle Q_b^{\nu'\mu} + \langle\sum_{a'}\frac{\partial k'(Q,e)}{\partial Q_{a'}}|_{Q=Q_0}|n(Q_0,e)\rangle Q_{a'}^{\nu'\mu}$$

(3.7)

where $Q_{a'}^{\nu'\mu}$ can be written as:

$$Q_{a'}^{\nu'\mu} = \langle\Theta^{\nu'}(Q)|Q_{a'}|\Theta^{\mu}(Q)\rangle$$

(3.8)

Considering the fact that most IETS experiments are performed at low temperatures, the initial vibration quantum number is assumed to be zero. The Eq. 3.8 can be calculated as $\sqrt{\frac{\hbar}{2\omega_{a'}}}$. Ignoring $\langle\sum_{a'}\frac{\partial k'(Q,e)}{\partial Q_{a'}}|_{Q=Q_0}|\sum_{b}\frac{\partial n(Q,e)}{\partial Q_b}|_{Q=Q_0}\rangle$, the Eq. 3.7 can be written as:

$$\langle\Theta^{\nu'}(Q)|\langle k'(Q,e)|n(Q,e)\rangle|\Theta^{\mu}(Q)\rangle = \langle k'(Q_0,e)|\sum_{b}\frac{\partial n(Q,e)}{\partial Q_b}|_{Q=Q_0}\rangle Q_b^{\nu'\mu}$$
$$+ \langle\sum_{a'}\frac{\partial k'(Q,e)}{\partial Q_{a'}}|_{Q=Q_0}|n(Q_0,e)\rangle Q_{a'}^{\nu'\mu}$$

(3.9)

Perform the same treatment for the other integral at the numerator of $g_{k',k}^{n,\nu',\mu,\nu}$, the Green's function can be written as:

$$g_{k',k}^{n,\nu',\mu,\nu} = \frac{(A+B)(C+D)}{E - E_n - \sum_a n_a\hbar\omega_a + i\Gamma_n}$$

(3.10)

23

where $A = \langle k'(Q_0, e)| \sum_b \frac{\partial n(Q,e)}{\partial Q_b}|_{Q=Q_0}\rangle Q_b^{\nu'\mu}$ and $B = \langle \sum_{a'} \frac{\partial k'(Q,e)}{\partial Q_{a'}}|_{Q=Q_0}|n(Q_0,e)\rangle Q_{a'}^{\nu'\mu}$. C and D are similar to B and A.

It is clear that the contribution to the current from the inelastic electron tunneling process can be included in the current by computing Green's function $g_{k',k}^{n,\nu',\mu,\nu}$. According to the definition of the inelastic electron tunneling spectroscopy (IETS), the IET spectrum can be obtained from $\frac{d^2 I_{DS}}{dV^2}$.

In our theoretical model, the conformation of the molecule remains unchanged when electrons tunnel through it. All the calculations are based on the ground state of the molecule and it is only adaptable in the weak e-p coupling condition with small bias applied (the normal IET spectra) and strong coupling between the molecule and electrode. More complicated phenomena such as the overtones appeared in IET spectra can not be explained with this low-order perturbation method. The popular NEGF method based on Born Approximation (BA) can be used to interpret the regular IETS, it is also can be extended to interpret the occurrence of the dip in IETS by including second-order e-p coupling. Both of them can not be interpreted with our model at the moment.

3.6   Spectra-conformation relationship

The sensitivity of the IETS is one of its advantages which is the basis to detect the detailed information in molecular junctions. In this section, we will discuss how these geometric properties influence the IET spectra by using our developed inelastic electron tunneling theory.

Electrode topography effect

One advantage of our theoretical method is that we can adopt different cluster models to simulate the interaction between the molecule and the electrode. The effect of electrode topography on the IETS can be seen from the following example. Here three kinds of electrode configurations are taken into account (see Fig. 3.4). Three gold atoms in a chain represent the sharp tip formed in the junction. The gold atoms in a triangle can simulate the relatively flat electrode. The tetrahedron configuration describes the situation between the chain shape and the triangle shape, with one gold atom in contact with the molecule and other three atoms in the plane of the second layer. Both ends of the molecule form chemical bond with the gold electrodes. The electrode distances for the three configurations are fixed as 1.036 nm. The directions of the molecule relative to the electrode are also the same.
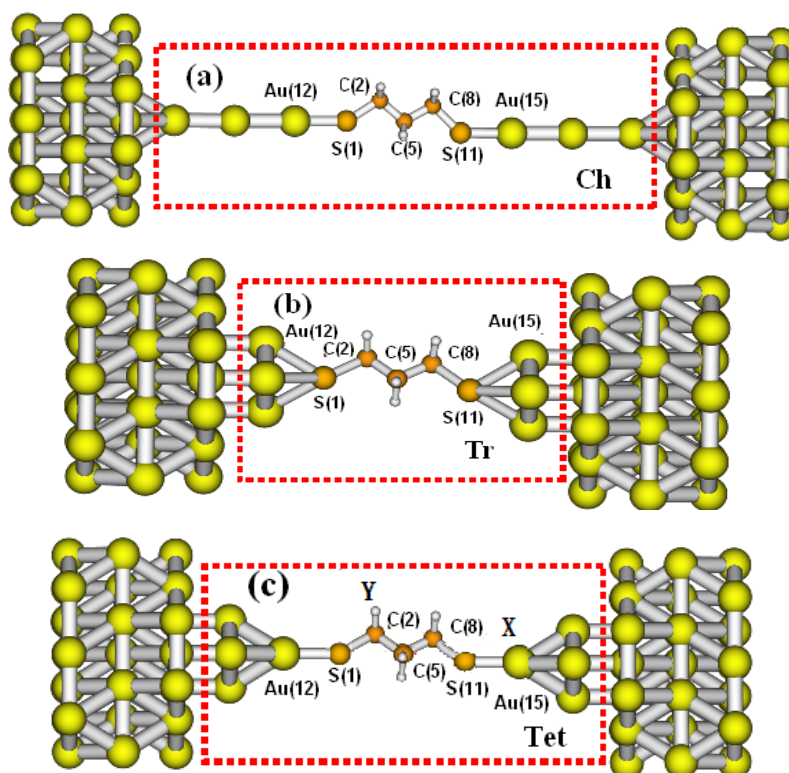
Figure 3.4: *Three different kinds of electrode configurations: (a) the "Ch" configuration with three gold atoms in a chain; (b) the "Tr" configuration with three gold atoms in a plane; and (c) the "Tet" configuration with four atoms in tetrahedron. The part in the frame is the extended molecule.* **Selected from Paper IV, adapted with the permission from the Journal of Physical Chemistry C, Copyright 2010, American Chemical Society.**

The calculated IET spectra of the three junctions are shown in Fig. 3.5. The IET spectra of the three configurations differ with each other significantly. The CH_2 symmetric scissoring vibration mode dominates the IET spectra of the "Ch" configuration. The vibration modes with lower frequencies such as C-S symmetric and antisymmetric stretching modes as well as the S-C-C symmetric scissoring mode are very weak in the IET spectra. The S-Au stretching mode shows the strongest signal in the IET spectra of "Tr" configuration. The CH_2 symmetric scissoring mode is not active in the IET spectra of this configuration. In general, the intensity of the vibration modes with low frequencies becomes stronger, while the opposite phenomenon is observed for the vibration modes with high frequencies. For the IES spectra of "Tet" configuration, the CH_2 symmetric scissoring

25
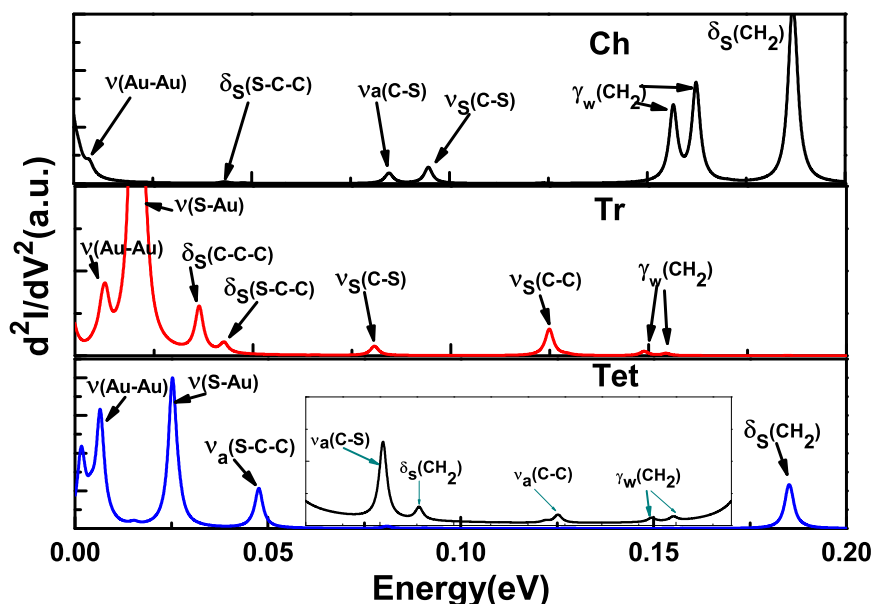
Figure 3.5: *IET spectra of the "Ch", "Tr" and "Tet" configurations. The central part in the IET spectra of "Tet" configuration has been amplified.* **Selected from Paper IV, adapted with the permission from the Journal of Physical Chemistry C, Copyright 2010, American Chemical Society.**

mode becomes active in the IET spectra again, the S-Au stretching mode become relatively weaker than that of "Tr" configuration. The intensity of the vibration modes in the middle of this figure has been amplified. Based on our calculations, we find that the sharp electrode tends to excite the vibration modes with higher frequencies, while the vibration modes with lower frequencies become more active when the electrode is flat. The similar phenomenon can also be found in our early calculations.[62] Of course, the influence of the electrode geometry on the IET spectra will mix with other impact factors, which makes the spectra-conformation relationship more complex.

Electrode distances effect

The effect of the electrode distances on the IET spectra is also quite significant, because it determines the coupling energy between the molecule and the electrode. Here the Benzenedithiol (BDT) molecule is investigated. The side view and the

26
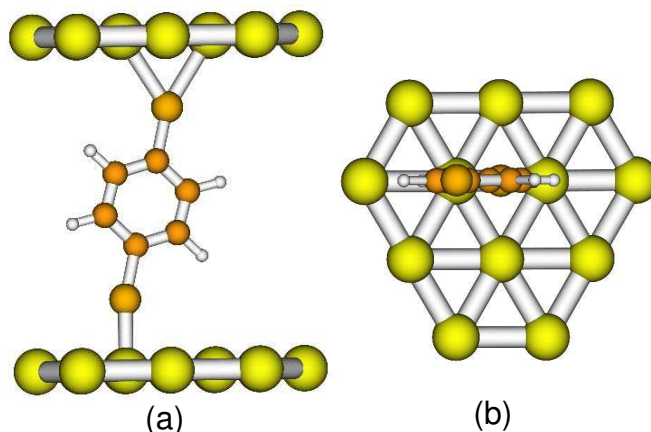
Figure 3.6: *Conformation of the Au_{12}-BDT-Au_{12} molecular junction investigated: (a) side view; (b) top view.*

top view of Au_{12}-BDT-Au_{12} molecular junctions are shown in Fig. 3.6. The anti-symmetric contact configurations are adopted with one sulfur atom located at the bridge site of the electrode while the other one located at the top site.

The calculated IET spectra of Au_{12}-BDT-Au_{12} with different electrode distances are shown in Fig. 3.7. When the electrode distance is small (1.09 nm and 1.17 nm), the vibration modes with low frequencies dominate the IET spectra. When the electrode distances are increased (1.25 nm and 1.33 nm), the vibration modes with high frequencies become more active, while the vibration modes with low frequencies become weak in the IET spectra. By careful assignment, the vibration modes around 0.05 V mainly come from the S-Au stretching vibration and the S-C stretching vibration. The vibration modes around 0.13 V come from the C-H bending modes ($\nu(19a)$ and $\nu(18a)$). As the electrode distances increase, the coupling interaction between the sulfur atom and the gold electrode becomes weak drastically, which induces the decreasing of the intensity of the S-Au stretching mode in the IET spectra. In general, all the intensity of the vibration modes will be weaken with the increasing of the electrode distances, while this effect is much more significant for the vibration modes from the end groups than those from the middle part of the molecule. Correspondingly, the intensity of vibration modes from the middle part of the molecule becomes to dominate the IET spectra when the electrodes is far away from each other to some extent.
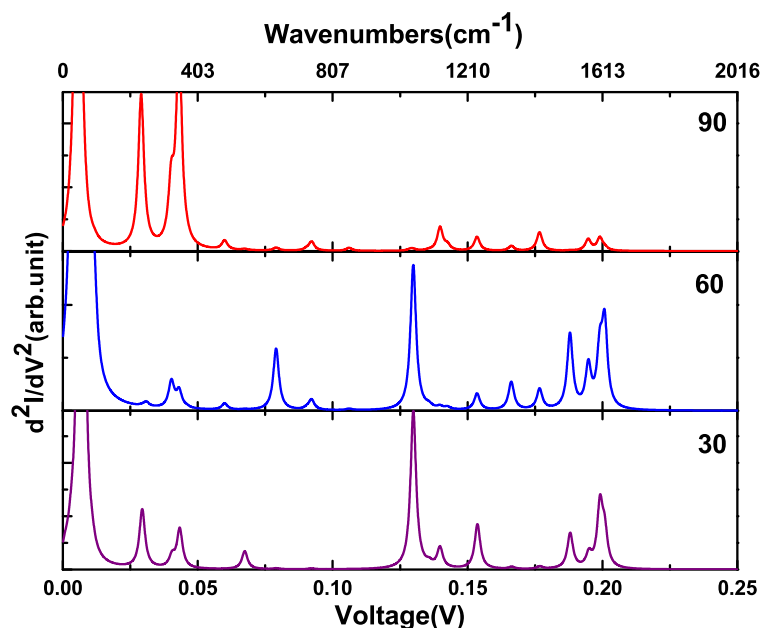
Rotation angles effect

Taking the conformation of the Au_{12}-BDT-Au_{12} molecular junction in Fig. 3.6 as a reference, we investigated the effect of the rotation angles of BDT molecule on the
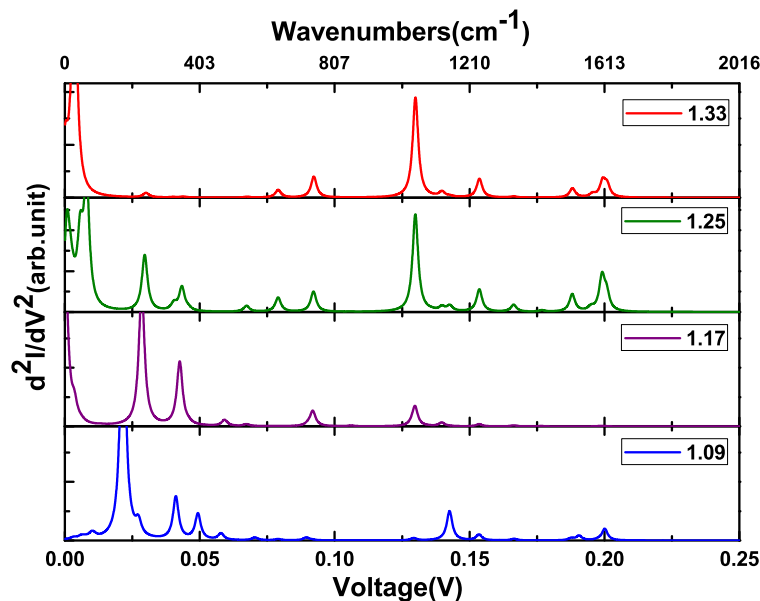
Figure 3.7: *IET spectra of the Au_{12}-BDT-Au_{12} molecular junction calculated with electrode distances 1.33 nm, 1.25 nm, 1.17nm and 1.09nm respectively.* **Selected from Paper II, adapted with the permission from ACS Nano, Copyright 2011, American Chemical Society.**

IET spectra. When the BDT molecule rotates around its S-S axis for 30, 60, and 90 degree respectively, the calculated IET spectra are shown in Fig. 3.8. Here the electrode distances are assumed as 1.25 nm. It is obvious that the IET spectra of the Au_{12}-BDT-Au_{12} molecular junction with rotation angle 30 and 60 degree are similar. The vibration modes with high frequencies are much stronger than those with low frequencies. There are more active vibration modes in the IET spectra at 60 degree than those in the IET spectra at 30 degree. The spectra profile of the molecular junction at 90 degree is significantly different from the other two. The S-Au vibration mode at the low frequencies area becomes to dominate the IET spectra, while the intensity of the vibration modes from 0.15 V to 0.2 V becomes very small. In this model, the rotation axis is not perpendicular to the electrode surface, therefore, when the molecule is rotated, the distances between the atoms of the molecule and the electrode will change, which will induce the variation of their coupling energies as well as the intensity of the vibration modes. However, if the rotation axis is perpendicular to the electrode surface, this rotation effect on the IET spectra will not be so significant.

Orientation effect

28

Figure 3.8: *IET spectra of Au$_{12}$-BDT-Au$_{12}$ molecular junctions with rotation angle 30, 60, and 90 degree respectively.*

The pathway based propensity rule comes from the investigation of the tile angles of the molecule relative to the electrode surface[134]. The tilt of the molecule can induce a new tunneling path opened. Taking the hexaecanethiol molecule (CH$_3$(CH$_2$)$_{15}$SH) as an example, the conformation of Au$_{12}$-CH$_3$(CH$_2$)$_{15}$S-Au$_{12}$ are shown in Fig. 3.9 (a). The angle β is the tilt angle which is defined as the angle between the S-C axis and the Y axis. When the S-C axis is located at the first quadrant, the value of β will be positive. If the S-C axis is in the second quadrant, its value will be negative. The IET spectra of Au$_{12}$-CH$_3$(CH$_2$)$_{15}$S-Au$_{12}$ with different tilt angles are shown in Fig. 3.9 (b). The IET spectra calculated at four configurations are different significantly. When the angle is 20 and 50 degree, there are no vibration modes active around 0.38 V. The IET spectra in the range of 0.075 V-0.2 V are also different with each other. When the tilt angle is -25 degree, the vibration mode around 0.38 V becomes active in the IET spectra. When β equals to -40 degree, the vibration mode around 0.38 V dominates the IET spectra. Calculated results indicate that this vibration peak around 0.38 V comes from the symmetric stretching vibration of the CH$_2$ groups close to the sulfur atom. When the tilt angle is -25 degree, the new tunneling path bypassing the end sulfur atom begins to open and compete with the original path through the sulfur atom. The symmetric stretching of the CH$_2$ group will favor the electron transport. When

29
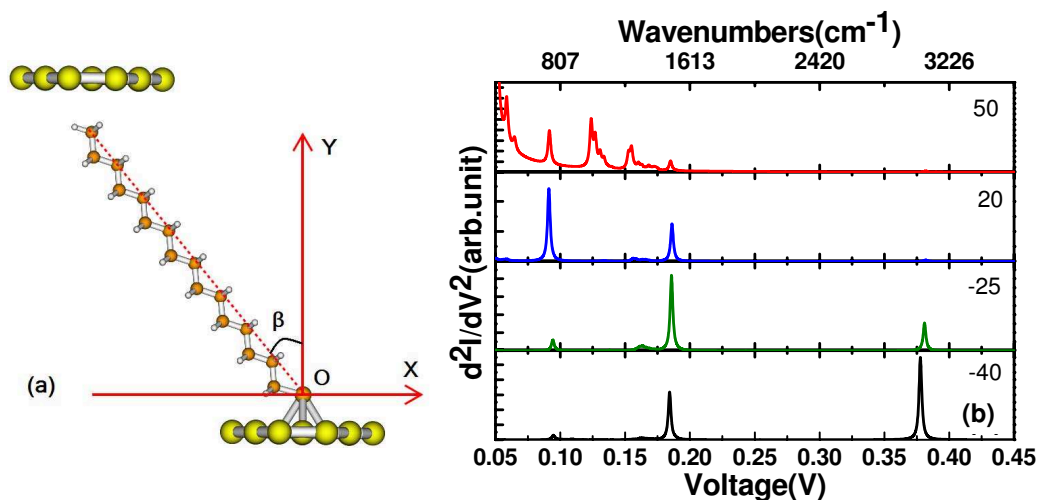
Figure 3.9: *(a) Conformations of Au_{12}-$CH_3(CH_2)_{15}S$-Au_{12} molecular junction; (b) IET spectra of Au_{12}-$CH_3(CH_2)_{15}S$-Au_{12} when the angle β is 50, 20, -25 and -40 degree respectively.* **Selected from Paper III, adapted with the permission from Journal of Physical Chemistry C, Copyright 2011, American Chemical Society.**

the tilt angle is -40 degree, the new tunneling path will be the main path, thus the CH_2 symmetric stretching mode will dominate the IET spectra.

In conclusion, the effect of some specific structure factors on the IET spectrum has been studied and some useful experience about the spectrum-conformation relationship has been obtained, although such a relationship is quite complicated because many structure factors can impose mixed effect on the IET spectrum. Besides these impact factors mentioned above, the interaction between molecules has also been indicated to have significant effect on the IET spectra[63].

Charge Transport in Organic Semiconductor Materials

4.1 Transport mechanism in organic semiconductor materials

In organic semiconductor materials, there are always two kinds of transport behaviors observed in experiments. One is that the charge mobility decreases with the increasing of temperatures, which is the typical characteristic in band transport mechanism. The other one is that the charge mobility arises as temperatures become higher, which is the proof of the hopping mechanism. In band transport, the charge carriers are described as a wavepacket with defined momentum and are scattered by lattices. The probability scattered increases as the temperature increases, thus smaller mobility is expected at the high temperature. In hopping mechanism, the carrier wavefunction is localized at one molecule and deforms the molecule (often called as small polarons). The transfer integral between two neighboring molecules is one of important factors to determine the charge mobility. According to the temperature dependent transfer integral,[138] it is easy to deduce that the charge mobility will decrease with the increase of the temperature. Although the temperature dependence can provide us the important information, the identification of the transport mechanism in organic materials is more complicated than we thought. Recently, Sirringhaus *et al.* investigated the temperature dependence of two kinds of pentacene derivatives, 6,13-bistriisopropyl-silylethynyl pentacene (TIPS-P) and 1,4,8,11-tetramethyl-6,13-triethylsilylethynyl pentacene (TMTES-P).[139] The band-like behavior has been found for the TIPS-P in low temperatures and the inverse tendency has been found in higher temperatures. Nevertheless, the charges optical response detected by charge modulation spectroscopy (CMS) indicated the existence of charges localized on the molecule. Shuai's group performed theoretical investigation on TIPS-P based on a localized picture and successfully reproduced the experimental results. It is indicated that organic semiconductor materials with the hopping mechanism can also preserve band-like behaviors. It is

necessary to seek better and effective way to determine the transport mechanism of organic semiconductor materials. With the great progress obtained in techniques, the detection of Hall mobilities in organic semiconductor materials have been increasingly popular because it is a better way to determine the transport regime by comparing with drift mobilities. It is widely accepted that the proof of the band transport is that the detected Hall mobility is as large as the drift mobility. For the organic materials with high mobilities such as rubrene and dinaphtho[2,3-b:2',3'-f]thieno[3,2-b]thiophene (DNTT), their Hall effect has been investigated and they have been proved to be band transport mechanism.[140]

4.2 Theoretical methods in hopping model

Early in the 1950s, Holstein have proposed the generalized theoretical method, namely the small polaron theory, to investigate the transport properties of organic molecular materials for both the hopping and band mechanisms mentioned above.[141,142] Here we focus on the small polaron hopping model and introduce the development in this model briefly. In Holstein model, only the intramolecular e-p coupling is considered. Based on the Holstein model, Munn and Silbey developed a variational approach and found that the non-local e-p coupling has the tendency to enhance the mobility in hopping mechanism.[143,144] In addition, Bobbert *et al.* extended the Holstein model by including the non-local e-p interaction to form the Holstein-Peierls model.[145–147] For a long period, semiclassic Marcus rate formula is the most popular method to investigate the charge transport properties in organic semiconductor materials. It has been combined with the quantum chemistry methods to calculate the parameters involved in the formula by *Brédas* and coworkers. While one should notice that this method is only valid at the high temperature limit ($\hbar\omega \ll K_B T$) and weak coupling conditions (the reorganization energy is much larger than the transfer integral). For generalization, Shuai's group developed the quantum-mechanical charge transfer rate equation which was previously derived by Jortner[148] and Lin[149] *et al.* and have been successfully applied in some systems.[75] In this thesis, the quantum charge transfer rate equation is adopted and the simple derivation is described. For details, we refer the work of Jortner[148] and Lin.[149]

Quantum-mechanic charge transfer rate is deduced from the Fermi Golden Rule. The transition rate from the initial state $|\psi_i\rangle$ to the final state $|\psi_f\rangle$ can be expressed as:

$$k_{fi} = \frac{2\pi}{\hbar^2} V_{fi}^2 \delta(E_{fi}),$$

(4.1)

where V_{fi} can be seen as the perturbation, here it is assumed as the interaction between two molecules and it can be written as:

$$V_{fi} = \langle \psi_f | V | \psi_i \rangle. \tag{4.2}$$

Here $|\psi_i\rangle = |\varphi_i \Theta_{iv}\rangle$ and $|\psi_f\rangle = |\varphi_f \Theta_{fv'}\rangle$, where $|\varphi_i\rangle$ and $|\varphi_f\rangle$ are electronic wavefunctions of the initial state and the final state, and $|\Theta_{iv}\rangle$ and $|\Theta_{fv'}\rangle$ are the vibration wavefunctions correspondingly. Since there are many vibration states in the initial state, the averaging for the initial state is performed and the distribution function for the vibration states obeying the Boltzmann distribution is expressed as:

$$P_{iv} = \frac{exp(\frac{-E_{iv}}{K_B T})}{\sum\limits_{v=1}^{\infty} exp(\frac{-E_{iv}}{K_B T})}, \tag{4.3}$$

where E_{iv} is the vibration energy of vibration state v in the initial state.

With Condon approximation, the charge transfer rate can be expressed as:

$$k_{fi} = \frac{2\pi}{\hbar^2} V_{fi}^2 \sum_{v,v'} P_{iv} |\langle \Theta_{fv'} | V | \Theta_{fv} \rangle|^2 \delta(E_{fv',iv}). \tag{4.4}$$

Here V_{fi} is the electron coupling between the initial state and the final state and $E_{fv',iv}$ is the energy difference between the initial state and the final state, which can be calculated as: $E_{fv',iv} = E_{fv'} - E_{iv}$.

In addition, based on the harmonic approximation, the vibration wavefunction

$$|\Theta_{iv}\rangle = \prod_{j} \chi_{iv_j}(Q_j), \tag{4.5}$$

where j is the label of vibration modes and $\chi_{iv_j}(Q_j)$ is the harmonic wavefunction. Correspondingly, the distribution function can be expressed as:

$$P_{iv} = \prod_{j} 2\sinh(\frac{\hbar\omega_j}{2K_B T}) \cdot \exp[\frac{-\hbar\omega_j(v_j + \frac{1}{2})}{K_B T}] = \prod_{j} P_{iv_j}. \tag{4.6}$$

The charge transfer rate can be expressed as:

$$k_{fi} = \frac{V_{fi}^2}{\hbar^2} \sum_{v_j} \sum_{v_{j'}} \prod_{j} \int dt \exp(iE_{fv_{j'},iv_j}t) P_{iv_j} |\langle \chi_{fv_{j'}} | \chi_{iv_j} \rangle|^2. \tag{4.7}$$

Here $\delta(E_{fv_{j'},iv_j})$ in Eq. 4.4 has adopted the integral expression under Fourier transformation and V_{fi} is designated as the transfer integral.

With the displaced harmonic oscillator approximation ($\Delta Q_j = Q'_j - Q_j$ and $\omega_{j'} = \omega_j$), the charge transfer rate can be finally written as:

$$k_{fi} = \frac{V_{fi}^2}{\hbar^2} \int_{-\infty}^{+\infty} dt \exp\{iE_{fi}t - \sum_j S_j[(1+2\bar{n}_j) - e^{i\omega_j t}(1+\bar{n}_j) - e^{-i\omega_j t}\bar{n}_j]\}. \quad (4.8)$$

Here E_{fi} is the potential energy difference between the final state and the initial state and ω_j is the vibration frequency of the vibration mode j. S_j is the Huang-Rhys factor, which can reflect the intensity of the e-p coupling, and it is defined as $S_j = \frac{\omega_j \Delta Q_j^2}{2\hbar}$. $\bar{n}_j$ is defined as $\frac{1}{e^{\frac{\hbar \omega_j}{K_B T}}-1}$.

For self-exchange reaction, the potential energy difference is zero, that is, $E_{fi} = 0$. When the e-p coupling is strong enough, with $\sum_{j=1} S_j \gg 1$, the short time approximation can be adopted.

$$e^{i\omega_j t} = 1 + i\omega_j t - \omega_j^2 t^2 \quad (4.9)$$

The quantum rate equation can be written as:

$$k_{fi} = \frac{V_{fi}^2}{\hbar^2} \int_{-\infty}^{+\infty} dt \exp\{-\sum_{j=1} S_j[(1+2\bar{n}_j)\omega_j^2 t^2 - i\omega_j t]\}. \quad (4.10)$$

When temperature is high with $\frac{\hbar \omega}{K_B T} \ll 1$, the rate equation can finally be written as:

$$k_{fi} = \frac{V_{fi}^2}{\hbar} \sqrt{\frac{\pi}{\lambda K_B T}} \cdot \exp(-\frac{\lambda}{4K_B T}). \quad (4.11)$$

This is the Marcus rate equation, where λ is the reorganization energy, and it is expressed as $\lambda = \sum_j S_j \omega_j \hbar$.

To obtained the so-called Bixon-Jortner rate, one mode with high frequency is dealt with the quantum method, while other modes will be treated classically based on the quantum rate equation. After these treatment, the rate can be written as:

$$k_{if} = \frac{V_{fi}^2}{\hbar^2} e^{-S_l(2\bar{n}_l+1)} \sum_{m_l=0}^{\infty} \sum_{n_l=0}^{\infty} \frac{(S_l \bar{n}_l)^{m_l}}{m_l!} \cdot \frac{[S_l(\bar{n}_l+1)]^{n_l}}{n_l!}$$
$$\frac{\cdot \exp[-\frac{\Delta E(m_l, n_l)}{K_B T} \cdot \frac{2\lambda' K_B T}{\sum'_{j=1} S_j(2\bar{n}_j+1)\omega_j^2}]}{\sqrt{\frac{\pi \hbar^2}{\lambda' K_B T} \cdot \frac{2\lambda' K_B T}{\hbar^2 \sum' S_j(2\bar{n}_j+1)\omega_j^2}}}. \quad (4.12)$$

where l is the mode with a high frequency, $\lambda' = \sum_{j}' s_j \omega_j \hbar$ is the reorganization energy without the contribution from the mode l and $\Delta E(m_l, n_l) = \frac{[\hbar\omega_l(m_l+n_l)+\lambda']^2}{4\lambda'}$.

When the temperature is very low with $\frac{\hbar\omega}{K_B T} \gg 1$, the rate equation will be

$$k_{if} = \frac{V_{fi}^2}{\hbar^2} e^{-S_l} \sum_{n_l=0}^{\infty} \frac{S_l^{n_l}}{n_l!} \cdot \exp[-\frac{\Delta E(0, n_l)}{K_B T}] \cdot \sqrt{\frac{\pi\hbar^2}{\lambda' K_B T}}. \tag{4.13}$$

This is the Bixon-Jortner rate equation.

Above derivation indicates that the quantum rate equation is more general than both the Marcus rate equation and the Bixon-Jortner rate equation. Normally the Marcus rate equation is only valid at the strong e-p coupling limit and the high temperature limit, while the Bixon-Jortner rate equation is applicable at the low temperature limit. Although Marcus rate equation has limited applicability, it can provide clear physical pictures and has been applied successfully to predict the transport properties of many organic materials as well as help one to design new materials with high mobility.

4.3 Parameter calculation

Benefited from the robust computational ability, it is possible to calculate the parameters involved in the rate equations. From the above three rate equations, we can see that the transfer integral (also called as electronic coupling) V_{fi} and the reorganization energy (λ) are two key parameters. The stronger the electron coupling is, the larger the charge transfer rate will be. The reorganization energy can also tell the e-p coupling intensity. The comparison of the two parameters can provide important and direct identification of the transport mechanism in the organic semiconductor materials. It is generally accepted that the hopping is the main mechanism in the materials with $V_{fi} \ll \lambda$ and the band transport happens in the materials with $V_{fi} \gg \lambda$. In addition, it can also help theoreticians to determine which method is suitable to investigate the transport properties of organic materials. Consequently, much effort has been devoted to improve the computational methods for these two parameters. Here we introduce some related methods

4.3.1 Transfer integral

In the above derivation of the quantum rate equation, the transfer integral is defined as the interaction between two states. For the electron transfer reaction, *e.g.*,

$A^- + B \Rightarrow A + B^-$, the initial state and the final state should be $|\psi(A^-)\psi(B)\rangle$ and $|\psi(A)\psi(B^-)\rangle$. Owing to the weak coupling between molecules in crystals and the ignorance of the multielectron effect, the two localized states can be approximately represented with one-electron molecular orbitals (LUMO for the electron transport and HOMO for the hole transport) of each monomer.

1. Direct coupling

In this method, the transfer integral is calculated as follows:

$$V_{AB} = \langle \psi_A \mid F \mid \psi_B \rangle \tag{4.14}$$

where ψ_A and ψ_B is the molecular orbitals of monomer A and B respectively. F is the Fock matrix of the dimers AB. At the level of DFT, F is the Kohn-Sham-Fock matrix and it can be calculated according to $F = SCEC^{-1}$. Here S is the overlap matrix, and C is molecular orbital coefficient matrix. This method has been used by Troisi's[150] and Shuai' group[75,151] et al.

2. Site energy correction

Considering the site energy correction, the transfer integral can be calculated according to:

$$V_{AB} = \frac{V_{AB}^0 - \frac{1}{2}(e_A + e_B)S_{AB}}{1 - S_{AB}^2} \tag{4.15}$$

where $V_{AB}^0 = \langle \psi_A \mid F \mid \psi_B \rangle$, $e_A = \langle \psi_A \mid F \mid \psi_A \rangle$ and $S_{AB} = \langle \psi_A \mid S \mid \psi_B \rangle$. This method was proposed by *Brédas et al.* and has been verified to be correct and useful.[152]

3. Energy splitting

Another simple method to evaluate the transfer integral is based on the Koopman's theorem and one-electron approximation.[153] It is designated that the electron coupling is half of the energy splitting between the frontier orbitals (LUMO or HOMO) of the dimer system. The transfer integral for holes can be calculated as:

$$V_{AB} = \frac{\epsilon_{HOMO} - \epsilon_{HOMO-1}}{2} \tag{4.16}$$

The transfer integral for electrons is calculated by:

$$V_{AB} = \frac{\epsilon_{LUMO+1} - \epsilon_{LUMO}}{2} \tag{4.17}$$

Attention should be paid when using this method. It is only valid when the molecules in the dimers are totally symmetric and closed shell systems.

Generally speaking, the Energy splitting method is much more crude than the other two methods, however, it can provide us a simple picture to understand

the electron coupling. Calculations have indicated that there is good agreement between the first two methods.[154]
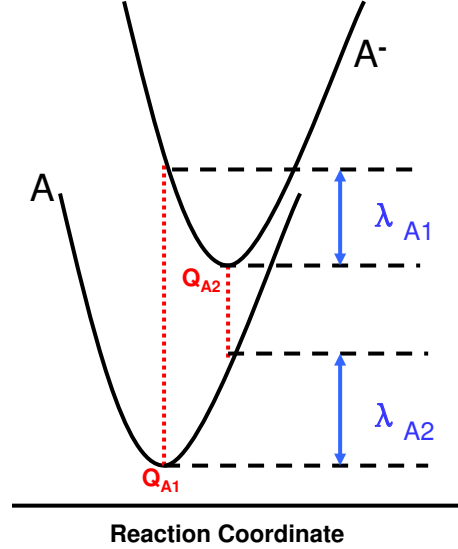
4.3.2 Reorganization energy

Reorganization energy is defined as the relaxation energy of one molecule from its initial state to its final equilibrium state when one electron is added in or removed away from it. We can understand this concept from an example. Take reaction $A^- + B \Rightarrow A + B^-$ as an example, where one electron transfers from molecule A to B. The reaction process can be understood from Fig. 4.1. Q_1 and Q_2 is the reaction coordinates of reactants and products in equilibrium. After the electron transfer from A to B, the equilibrium position has changed. Suppose that the atomic coordinates do not change as soon as the electron is transferred, the products will located at a high energy level. After the relaxation, the products go back to the equilibrium. The energy difference λ_1 between the energy of the products at Q_1 and Q_2 is defined as the reorganization energy of the reaction. Correspondingly, λ_2 is the reorganization energy of the reverse reaction. Generally, the reorganization energy of this reaction is taken as the average of λ_1 and λ_2. In particular, λ_1 will equal to λ_2 for self-exchange reactions.
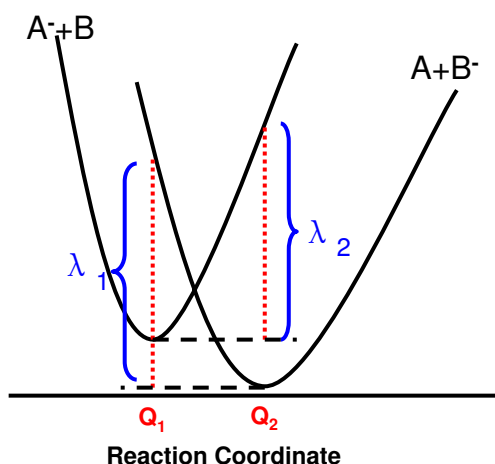
Figure 4.1: *Reorganization energy reflected in the reaction coordinate.*

Since the interaction between A and B is weak, its influence on the configuration relaxation of A and B can be neglected. Consequently, the reorganization energy can be simplified as the sum of λ_A and λ_B. λ_A is the relaxation energy of A from anion state to neutral state (see Fig. 4.2), and it can be calculated as: $\lambda_A = \frac{\lambda_{A1} + \lambda_{A2}}{2}$. λ_B can be obtained by the same way. It is also very easy

to deduce that the reorganization energy for the self-exchange reaction such as $A^- + A \Rightarrow A + A^-$ is $2\lambda_A = \lambda_{A1} + \lambda_{A2}$.

Figure 4.2: *Simplified reorganization energy representation.*

Based on the above definition, there are two kinds of methods to calculate the reorganization energy for the self-exchange reaction. One is called as the Four Site Energy method or Adiabatic Potential Energy method, and the other one is based on the analysis of normal vibrations modes. The two methods have been proven to agree with each other very well.

1. Adiabatic Potential Energy Surface (Four-site Energy)

As is shown in Fig. 4.2, to calculate the reorganization energy of λ_{A1} and λ_{A2}, one has to calculate the potential energy at four sites. For convenience, we define two potential energy functions $E_A(R)$ and $E_{A^-}(R)$ where R is the reaction coordinate. $E_A(R)$ and $E_{A^-}(R)$ are the potential energy functions for the neutral and the anion system respectively. It is direct to obtain:

$$\lambda_{A1} = E_{A^-}(Q_{A1}) - E_{A^-}(Q_{A2}) \tag{4.18}$$

$$\lambda_{A2} = E_A(Q_{A2}) - E_A(Q_{A1}) \tag{4.19}$$

The reorganization energy can be calculated as $\lambda = \lambda_{A1} + \lambda_{A2}$.

2. Normal Mode Analysis

38

It was proposed by Reimers that the reorganization energy can be projected on all the vibration modes:[155]

$$\lambda = \sum_{i=1} \lambda_i = \sum_{i=1} \frac{1}{2} F_i \Delta Q_i^2 = \sum_{i=1} \frac{1}{2} \omega_i^2 \Delta Q_i^2 = \sum_{i=1} \hbar S_i \omega_i \qquad (4.20)$$

where F_i is the force constant of the system, ΔQ_i is the displacement between the equilibrium neutral configuration and the anion configuration along the vibration mode i, and ω_i is the vibration frequency of the vibration mode i. From above equations, one can also notice that there is a tight correlation between the reorganization energy and the Huang-Rhys factor.

4.4 Charge mobility
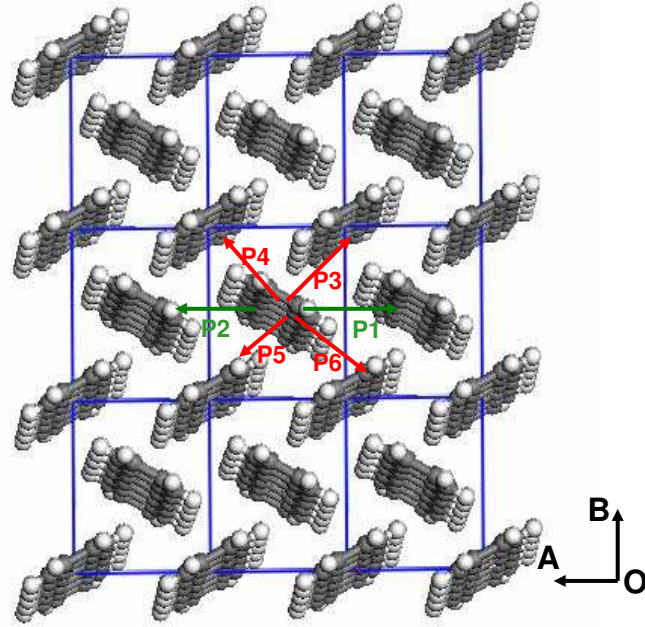
Figure 4.3: *All possible charge transport pathways on the surface of AOB of the pentacene single crystal.*

When all the parameters are obtained in the rate equation, the charge transfer rate is ready to calculate. For the convenience of comparison with experimental results, the macro physical quality, charge mobility, should be calculated theoretically. To the best of my knowledge, two approaches have been employed to calculate the charge mobility. One is based on the master equation, in which method the carrier

density and electronic field effect can be investigated. This approach has been successfully applied on the polymer systems[156] as well as small molecule systems.[157] The other approach is the Kinetic Monte Carlo method, which is good for simulating the diffusion mobility.[75,151] Of course, it also can be approximately applied to calculate the drift mobility when the electronic field is very weak.
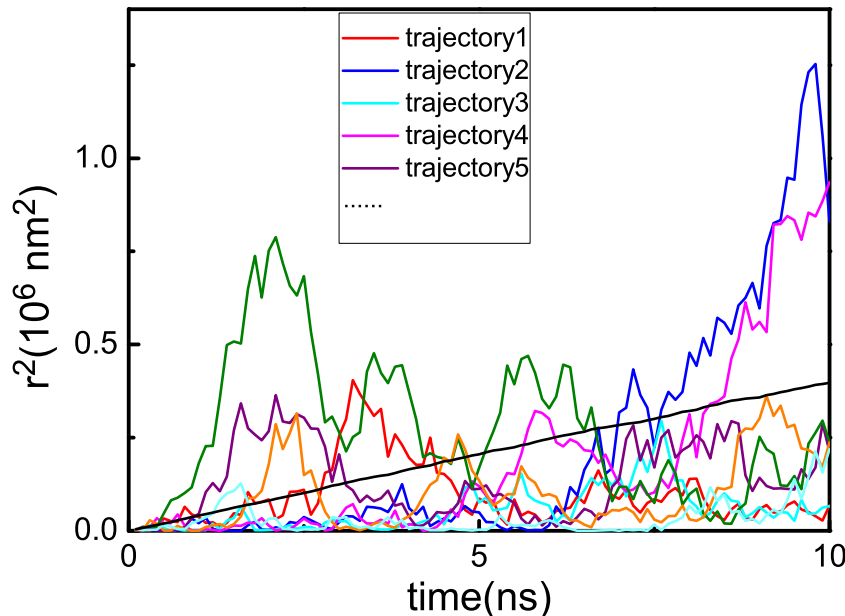
Figure 4.4: *The square of the charge transport displacement verse time. The black line is the average on thousands of records.*

Here I simply introduce the general procedure to compute the charge mobility by the random walk method. Taking the pentacene molecule as an example, its crystal structure viewed from the C axis is shown in Fig. 4.3. On the AOB plane, there are six neighbors for every molecule. It means there are six pathways for electrons to transfer from one molecule if we ignore the transport along C axis (see Fig. 4.3), and the probability to transport through Pi is $W_i = \frac{k_i}{\sum_{i=1}^{N} k_i}$. Correspondingly, the hopping time is $\frac{1}{k_i}$, where k_i is the charge transport rate along Pi. Based on the rate equation mentioned in Section 2, one can get the transport probability through all the pathways. Then we perform the random walk simulation. Suppose one charge is located at any one molecule, then a random number W is generated by the computer, and it is compared with the probability distribution

of every pathway. If $\sum\limits_{i=1}^{i=j-1} W_i < W < \sum\limits_{i=1}^{i=j} W_i$, the charge will transport through Pj to the second molecule. When the charge is located at the second molecule, a new random number will be generated and a new pathway will be decided according to the above mentioned criteria. Eventually the charge transport trajectory will be obtained. For example, the transport trajectory can be exported every 10 ns. By thousands of similar simulations, lots of tracks are obtained. The average on the thousands of records can give the linear relationship between the square displacement r^2 and the diffusion time t though the single record is completely irregular (see Fig. 4.4). The definition of the diffusion coefficient is as follows:

$$D = \lim_{t \to \infty} \frac{r^2}{2nt} \tag{4.21}$$

Where r and t is the total displacement and time for every track. n is the dimension parameter. Consequently, the charge mobility can be calculated with the Einstein equation:

$$\mu = \frac{eD}{K_B T} \tag{4.22}$$

It should be stressed that the mobility calculated here is the diffusion mobility for which there is no electronic field added. If one adds the weak electronic field, the drift mobility can be approximated by the calculation of the diffusion mobility. The only difference between them is to consider the potential energy difference $(-e\vec{r}\cdot\vec{E})$ between two neighbor sites induced by the electronic field. For the strong electronic field, the random walk approach is thus not a reasonable approach.

Summary of Included Papers

In this chapter, a brief summary of my papers included in the thesis and our contributions to the research field will be presented.

5.1 Elastic electron transport properties, Paper I

The study on elastic electron transport properties of molecular junctions has been very intensive both experimentally and theoretically in the last two decades. The transport mechanism was verified as the tunneling process in most small molecular junctions. Although the conformation of the molecular junction can not be determined experimentally, some impact factors such as the molecular length, molecular components, substitution groups, anchor groups, contact positions, electrode materials, the solvent effect and so on, have been systematically studied. However, the effect of aromatic coupling on the transport properties of molecular junctions was rarely investigated. It was commonly thought that the preparation of single molecular junctions with Break Junction method is impossible if the target molecule has only one anchor group. However, in 2008, Wu *et al.* reportd an experimental study that showed two molecules could be coupled together to form bimolecular junctions through the aromatic coupling.[129] Right after that, we performed theoretical investigation on the aromatic effect.

For the nitrogen substituted OPE molecule, there are two kinds of parallel stacking conformations: the para-conformation and the ortho-conformation (see Fig. 5.1). In our model, each molecule is connected with one electrode, and the electrons can only tunnel from one electrode to one molecule, then jump to the other molecule and at last tunnel to the electrode on the other side. Based on the energy calculation, the ortho-conformation was proven to be more stable than the
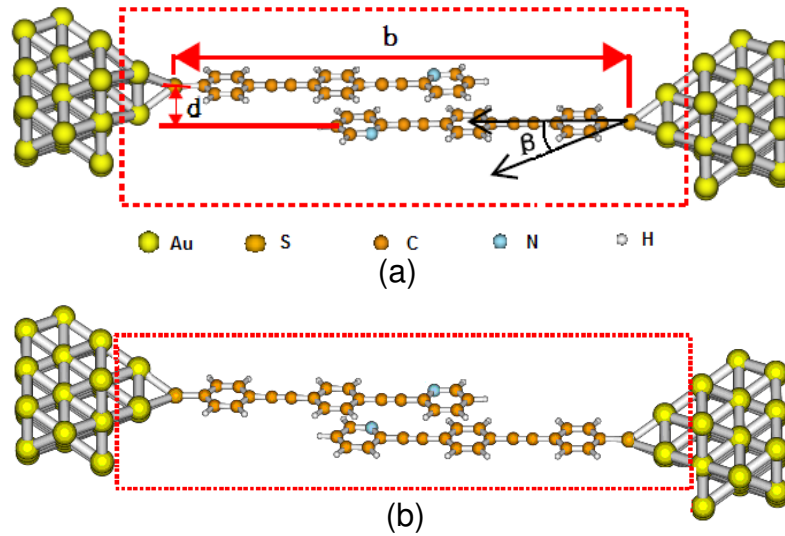
Figure 5.1: *Conformations of nitrogen substituted OPE bimolecular junction investigated: (a) ortho-conformation; and (b) para-conformation. The dashed frame contains the extended molecular system. Parameter b and d represent the lateral and vertical distance, β is the tilt angle of the lower molecule relative to the upper one.* **Selected from Paper I, reprinted with permission from Journal of Physics: Condensed Matter, Copyright 2010, Institute of Physics.**

para-conformation, thus our theoretical investigations were all performed on the ortho-conformation.

Our calculations indicated that the coupling between two molecules in the junctions is determinant for the formation of bimolecular junctions. The weakening of the coupling energy between two molecules can induce the decrease of the conductance of bimolecular junctions. When the vertical distance (d) decreases from 0.34 nm to 0.28 nm, the coupling energy increases to 7.078 eV from 0.780 eV. The calculated conductance-voltage curves are shown in Fig. 5.2 (a). The conductance values on the plateau become larger with d decreasing. The conductance-voltage curves of the bimolecular junctions with different horizontal distances (b) are shown in Fig. 5.2 (b). Here b1 and b2 represent the conformations with b=2.17 nm and 3.56 nm respectively. The black line is the conductance curve of the conformation with b=2.88 nm (b0). It is obvious that the conductance values on the plateau reduce with the horizontal distance increasing. The coupling energy between two molecules for b1, b0 and b2 are 3:2:1, which is consistent with the overlapping benzene rings. The deviation between two molecules can also weaken the coupling

as well as the conductance ability (see Fig. 5.2 (c)). A and B represents the conformations that there are 0.12 nm and 0.24 nm slide between two molecules along the short axis direction respectively. With the deviation increasing, the conductance values at the plateau are also reduced. There are also 31% and 71% decrement in the coupling energy compared with that of b0. Our calculation also indicated that the coupling energy and conductance values are very sensitive to the tilt angles (β) (see Fig. 5.2 (d)). A small tilt angle will induce drastic decrease of the coupling energy and conductance values. When the tilt angle is larger than 5 degree, the conductance become so small that it will be very difficult to be detected. This will provide the proof that the formation of bimolecular junctions should be based on the parallel configurations.
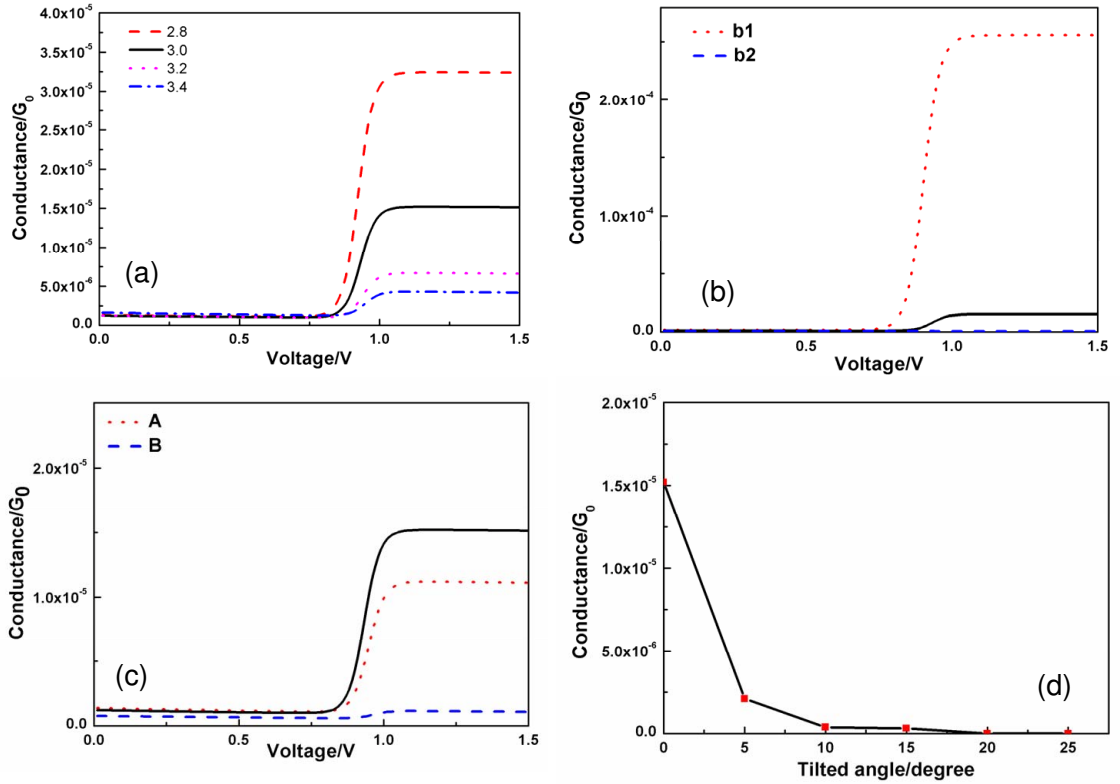
Figure 5.2: *Conductance-voltage curves of the bimolecular junction with different vertical distances (a), horizontal distances (b) and deviations (c). The black curve in (a), (b) and (c) are calculated with b=2.88 nm and d=3.0 nm. (d) The conductance values calculated at 1.0 V bias with different tilt angles.* **Selected from Paper I, adapted with the permission from Journal of Physics: Condensed Matter, Copyright 2010, Institute of Physics.**

5.2 Inelastic electron tunneling spectra, Paper II-IV

The study of inelastic electron tunneling spectroscopy is very active in the last ten years. Owing to its peculiar characteristics, it has become the primary technique to study the structures in molecular junctions. Many typical systems, like conjugated and alkane systems, have been intensively studied. However, experimental spectra can not tell us the structural information we need without the support of theoretical simulations and interpretation. In this thesis, we selected some typical systems: the 1,4 benzenedithoil molecule, a serial of semifluorinated hexadecanethiol molecules and the 1,3-propanedithiol molecule, to study their inelastic transport properties. Some pendent questions that emerged recently or confused for years in this area have been successfully resolved.

5.2.1 Conjugated system, Paper II

In spite of intensive studies by different groups, the reported conductance values of 1,4 benzenedithoil (BDT) molecular junctions vary in almost 4 orders of magnitude, and its uncertainty of contact configurations in the junctions is thought to be the main impact factor. In 2009, Song *et al.* and Tsutsui *et al.* performed IETS on BDT molecular junctions using the electromigrated nanogap method and the mechanically controllable break junction (MCBJ) method respectively and obtained four different spectral profiles.[158–161] To find out what has caused such big differences in the IETS of the same molecule, we then performed systematic investigation on the 1,4 benzenedithoil molecular junctions (Au_{12}-BDT-Au_{12}). The experimental spectra detected by the two groups mentioned above have been successfully reproduced (as illustrated in Fig. 5.3). The upper two red curves are the experimental spectra detected by Song' group[158,161] using the electromigrated nanogap method, while the lower two red curves are obtained by the Tsutsui *et al.*[159,160] with the MCBJ method. The different molecular conformations in the junctions prepared by different techniques are found to be the major source for the spectral difference. Our calculations indicated that the upper two conformations of the molecular junctions adopt the same contact style with the same electrode distance. The only difference lies in the molecular rotation angle. The deviations between the lower two conformations are much more significant. One adopts an asymmetric contact manner, while another has a symmetric contact style. The latter is much narrower than the former. Consequently, it suggests that the electromigrated nanogap method is more reproducible than the MCBJ technique.
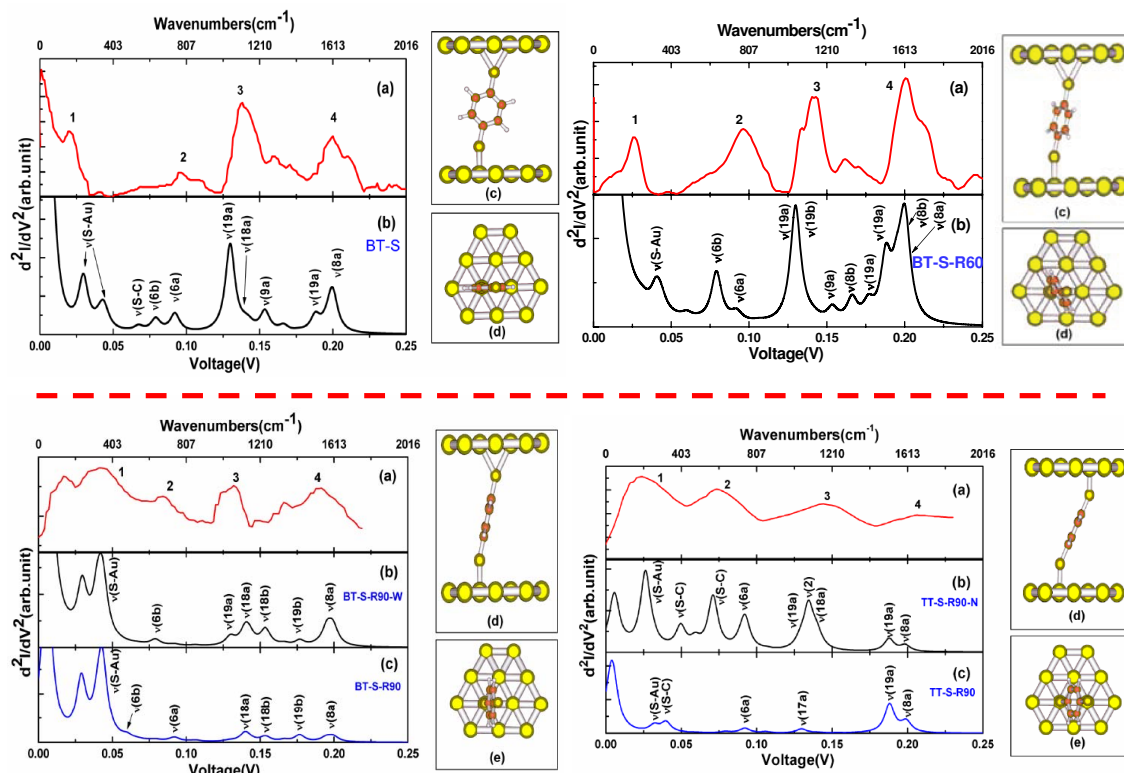
Figure 5.3: *Comparison between calculated IET spectra (black curve) and the experimental counterparts (red curve). The conformations of the molecular junctions calculated are also presented.* **Selected from Paper II, adapted with the permission from the ACS Nano, Copyright 2011, American Chemical Society.**

5.2.2 Alkane systems, Paper III-IV

For the inelastic electron tunneling spectra of alkanethiol molecules, two problems were still not resolved. Theoretical simulations failed to reproduce the dominant character of the C-H stretching mode at about 0.36 V in the IET spectra. The other problem is that the origin of the C-H stretching vibration mode is still in controversy. Most theoretical studies assigned it to come from the CH_3 group.[58,162] Beebe *et al.* proved that it should come from the CH_2 groups close to the sulfur atom by gradually fluorinating the CH_3 group and CH_2 groups close to it.[163] In 2010, it was also stated that it might belong to both the CH_3 group and CH_2 group involving both symmetric and antisymmetric modes.[164] By a systematic study on the IET spectra of a serial of semifluorinated hexadecanethiol molecules,

we successfully reproduced the experimental IET spectra detected by Beebe and co-workers. Based on our reliable simulations, the origin of the C-H stretching mode has been confirmed as coming from the CH_2 groups close to the sulfur atom. In addition, the calculated results showed that the contact pattern as well as the tilt angles of the molecule relative to the electrode are two important factors that can influence the intensity of the C-H stretching mode. When the molecule is tilted -40 degree and both the end sulfur and carbon atoms are located at the hollow sites of the electrodes, the C-H stretching mode can dominate the IET spectra. At this condition, a new tunneling path bypassing the end sulfur atom can open, which makes the C-H stretching mode more significant for electrons to transport (see Fig. 5.4) and dominant in the IET spectra. Our calculations strongly supported the pathway based propensity rule proposed by Troisi and Ratner.[134]
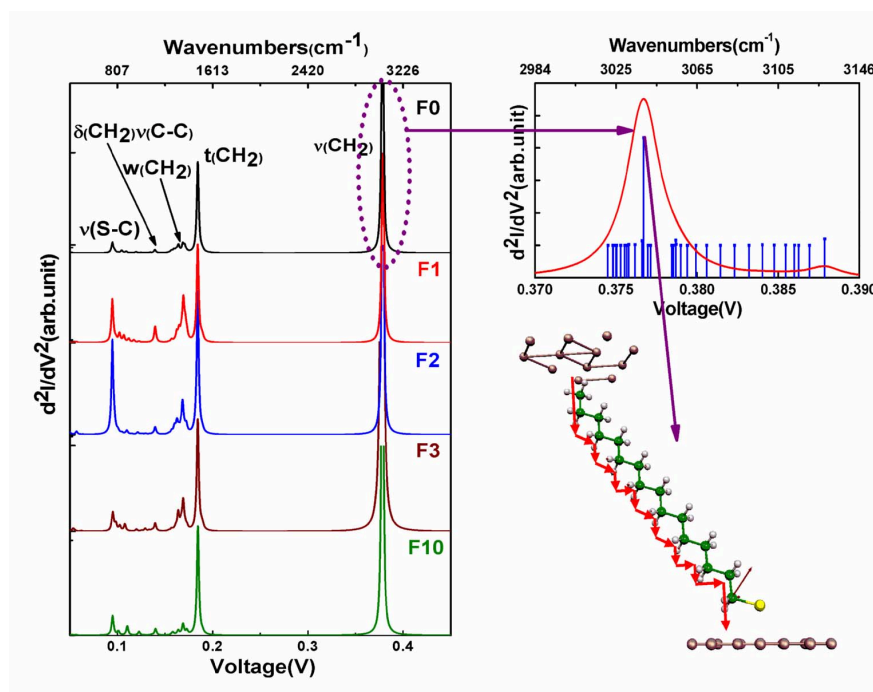
Figure 5.4: *Calculated IET spectra of semifluorinated molecular junctions and the detail vibration modes at about 0.38 V. The C-H stretching modes and the new tunneling path (red arrows) is shown at the bottom of right side.* **Selected from Paper III, reproduced with the permission from the Journal of Physical Chemistry C, Copyright 2011, American Chemical Society.**

For 1,3-propanedithiol molecular junction, two significantly different IET spectra were obtained experimentally.[165] Our simulations have successfully reproduced both experimental spectra. It is found that the IET spectra are sensitive to the tilt

angles of the molecular chain relative to the gold surface. The differences between two IET spectra detected are attributed to the different tilt angles between two molecular junctions.
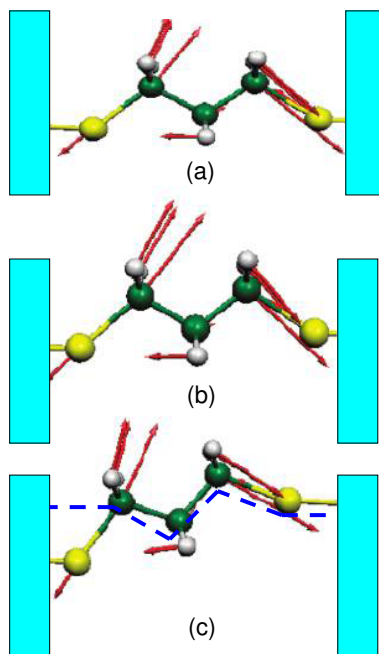
Figure 5.5: *(a) (b) and (c) are the vibration profiles of ν_a(S-C) when tilt angle β is 0, 10, and 25 degree respectively. The blued dashed line represents the new tunneling path.* **Selected from Paper IV, adapted with the permission from the Journal of Physical Chemistry C, Copyright 2010, American Chemical Society.**

One should pay attention to the ν_a(S-C). The appearance of the antisymmetric stretching modes in the IET spectrum is not allowed according to the propensity rule proposed by Troisi *et al.*[136] However, exception may exist when the molecule is very small that many tunneling paths can coexist. When the molecule is tilted relative to the electrode, the new tunneling path bypassing the end sulfur atom opens and competes with the original path where both the end sulfur atoms are involved (as shown in Fig. 5.5). When the angle is 0 and 10 degree, the carbon atom close to the sulfur atom is far away from the electrode. However, when the tilt angle is 25 degree, the carbon atom gets close to the electrode and can couple with the electrode strongly, then the new tunneling pathway may open (see the blue dashed line in (c)). Thus the quasi-antisymmetric vibration mode shows its

significant contribution to the IET spectra. Our calculation directly confirmed the tunneling path based propensity rule proposed by Troisi *et al.*[134]

5.3 Charge transport in organic semiconductor materials, Paper V

The transport mechanism in organic molecular materials is totally different from that in molecular junctions. The electrons in organic molecular materials jump from one molecule to another, and can stay at the molecule long enough to induce the relaxation of the molecular geometry. This kind of transport is defined as the hopping process.
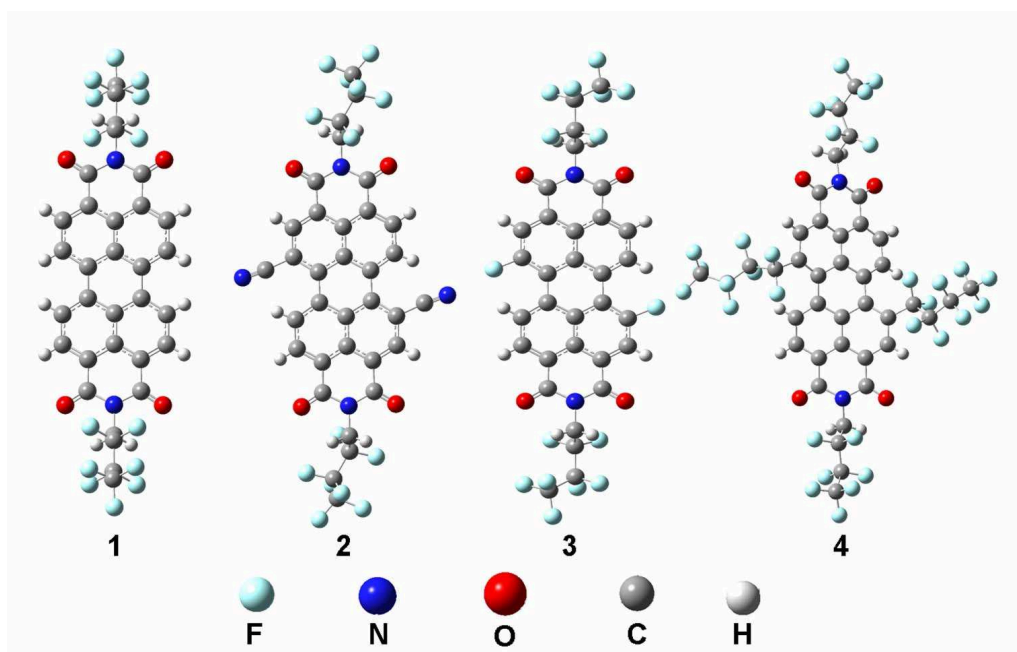
Figure 5.6: *Systems investigated and their configurations in crystal phase.*

In organic molecular materials, the hole transport properties of p-type materials have been intensively studied. However, the n-type materials were much less investigated due to their low charge mobilities and poor solubility. Nevertheless, it is necessary to pay more attention to the n-type materials for the completeness of the circuit. Recently, many n-type organic materials have been found to have large mobilities comparable with the amorphous silicon material. One of the them is the N,N'-bis(n-alkyl)-(1,7 and 1,6)-dicyanoperylene-3,4:9,10-bis(dicarboximide) (PTCDI) with $CH_2C_3F_7$ group as the end substitution (PDIF-CN2).[104,166–168] To investigate how the substitution groups on the bay positions influence the transport

properties in organic materials, four kinds of n-type organic single crystal materials were investigated by employing the quantum rate equation combined with the random walk approach (see Fig. 5.6). The substitutions at the bay positions of the PDI molecule not only induce the change of geometric structures and the electronic structures, more importantly, the reorganization energy and the stacking patterns in the organic crystal materials are drastically influenced. Calculations indicated that the cyano group is a preferable substitution group which can both reduce the reorganization of the molecule and increase the transfer integral. Substitutions with long perfluoroalkane chains are found to be not good, since they can increase the reorganization energy and induce larger barriers for the charge to transport due to the long distance segregation of the molecules in the crystals.
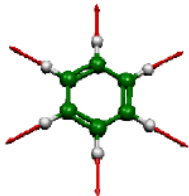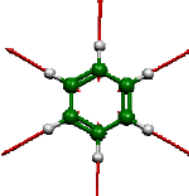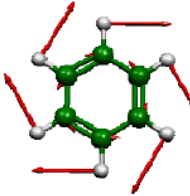
In conclusion, three kinds of transport processes including elastic, inelastic and hopping processes in molecular systems have been investigated and some specific phenomena have been explained successfully. As mentioned at the beginning of this thesis, the charge transport process in molecular systems is much more complex. Many phenomena such as Coulomb blockade and Kondo resonance are beyond the scope of our current methods. Progress along these directions has been made recently. The noise of the current, the heating and even the spectroscopy under the illumination are the central issues for molecular junctions. For the charge transport in organic semiconductors, the determination of the transport mechanism is still in controversy even though the Hall mobility measurement can provide us relatively reliable way. In any case, more sophisticated theoretical and computational methods need to be developed to meet all the challenges.
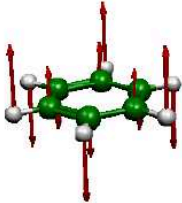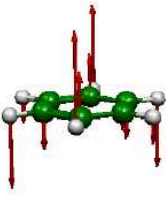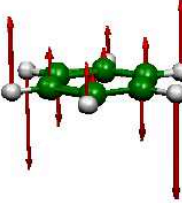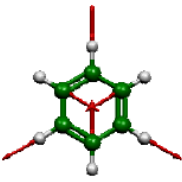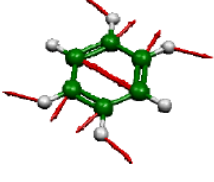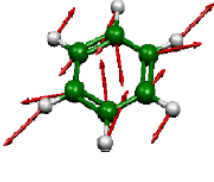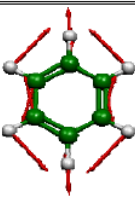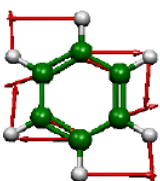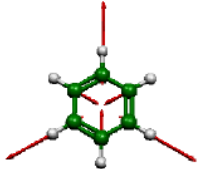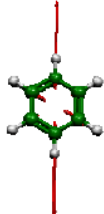
Appendix

According to the vibration characteristics of the benzene molecule, its 30 vibration modes can be classified into nine groups. The first three groups include only one vibration mode for each kind (see Fig. 5.7). Three vibration modes are involved for the "Ring Torsion Mode", the "C-C-C Bending Mode" and the "C-C Stretching Mode" respectively (see Fig. 5.8). There are five vibration modes for the "C-H Stretching Mode" (see Fig. 5.9), six vibration modes for the "C-H out-of-plane Wagging Mode" (see Fig. 5.10) and seven vibration modes for the "C-H Bending Mode" (see Fig. 5.11). The frequencies are calculated in `Gaussian 03` program with B3LYP functional and 6-31G* basis set.

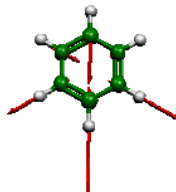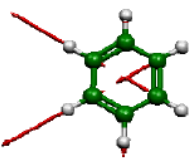| Vibration Modes			
Label	1	2	3
Frequency (cm^{-1})	1022.17	3226.90	1420.70
Name	Breathing Mode	Beat Mode	Twist Mode

Figure 5.7: *Vibration pictures, labels and frequencies for three kinds of vibration modes of benzene molecule.*

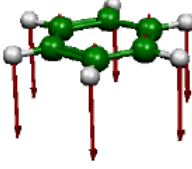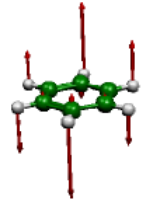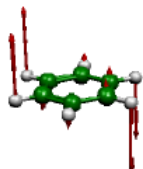| Ring Torsion Modes			
Label	4	16a	16b
Frequency (cm^{-1})	737.74	442.10	442.10
C-C-C Bending Modes			
Label	12	6a	6b
Frequency (cm^{-1})	1049.10	639.85	639.85
C-C Stretching Modes			
Label	15	8a	8b
Frequency (cm^{-1})	1366.83	1541.80	1541.80

Figure 5.8: *Vibration pictures, labels and frequencies for the "Ring Torsion Mode", the "C-C-C Bending Mode" and the "C-C Stretching Mode" of benzene molecule.*

54

C-H Stretching Modes			
Label	13	7a	7b
Frequency (cm^{-1})	3184.47	3194.42	3194.42
C-H Stretching Modes			
Label	20a	20b	
Frequency (cm^{-1})	3212.62	3212.62	
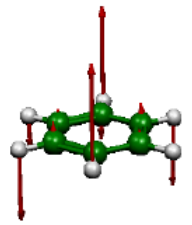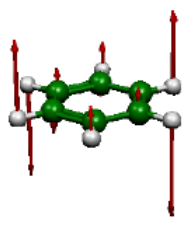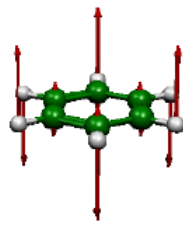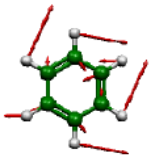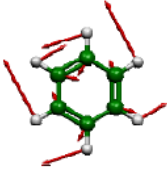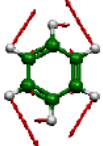
Figure 5.9: *Vibration pictures, labels and frequencies for the "C-H Stretching Mode" of benzene molecule.*

55

C-H Out of Plane Wag Modes			
Label	11	10a	10b
Frequency (cm^{-1})	705.85	884.44	884.44
C-H Out of Plane Wag Modes			
Label	17a	17b	5
Frequency (cm^{-1})	1000.85	1000.85	1045.10

Figure 5.10: *Vibration pictures, labels and frequencies for the "C-H out-of-plane Wagging Mode" of benzene molecule.*

C-H Bending Modes			
Label	14	18a	18b
Frequency (cm^{-1})	1218.31	1077.90	1077.90
C-H Bending Modes			
Label	19a	19b	9a
Frequency (cm^{-1})	1541.80	1541.80	1232.30
C-H Bending Modes			
Label	9b		
Frequency (cm^{-1})	1232.30		

Figure 5.11: *Vibration pictures, labels and frequencies for the "C-H Bending Mode" of benzene molecule.*

57

REFERENCES

[1] A. Aviram and M. Ratner, Chem. Phys. Lett, **29**(2), 277–283, 1974.

[2] M. Reed, C. Zhou, C. Muller, T. Burgin, and J. Tour, Science, **278**(5336), 252, 1997.

[3] C. Muller, J. Van Ruitenbeek, and L. De Jongh, Physica C: Superconductivity, **191**(3-4), 485–504, 1992.

[4] J. Krans, C. Muller, I. Yanson, T. Govaert, R. Hesper, and J. Van Ruitenbeek, Physical Review B, **48**(19), 14721–14724, 1993.

[5] C. Untiedt, M. Caturla, M. Calvo, J. Palacios, R. Segers, and J. Van Ruitenbeek, Physical Review Letters, **98**(20), 206801, 2007.

[6] B. Ludoph and J. Ruitenbeek, Physical Review B, **61**(3), 2273–2285, 2000.

[7] D. Bakker, Y. Noat, A. Yanson, and J. Van Ruitenbeek, Physical Review B, **65**(23), 235416, 2002.

[8] S. Nielsen, M. Brandbyge, K. Hansen, K. Stokbro, J. Van Ruitenbeek, and F. Besenbacher, Physical Review Letters, **89**(6), 66804, 2002.

[9] J. Reichert, R. Ochs, D. Beckmann, H. Weber, M. Mayor, and H. Lohneysen, Physical Review Letters, **88**(17), 176804, 2002.

[10] R. Huber, M. GonzÍćlez, S. Wu, M. Langer, S. Grunder, V. Horhoiu, M. Mayor, M. Bryce, C. Wang, and R. Jitchati, J. Am. Chem. Soc, **130**(3), 1080–1084, 2008.

[11] M. Gonzalez, S. Wu, R. Huber, S. Van Der Molen, C. Schonenberger, and M. Calame, Nano Letters, **6**(10), 2238–2242, 2006.

[12] L. Bumm, J. Arnold, M. Cygan, T. Dunbar, T. Burgin, L. Jones, D. Allara, J. Tour, and P. Weiss, Science, **271**(5256), 1705, 1996.

REFERENCES

[13] N. Tao, Physical Review Letters, **76**(21), 4066–4069, 1996.

[14] X. Cui, A. Primak, X. Zarate, J. Tomfohr, O. Sankey, A. Moore, T. Moore, D. Gust, G. Harris, and S. Lindsay, Science, **294**(5542), 571, 2001.

[15] N. Agrait, J. Rodrigo, and S. Vieira, Physical Review B, **47**(18), 12345–12348, 1993.

[16] J. Pascual, J. Mendez, J. Gomez-Herrero, A. Baro, N. Garcia, U. Landman, W. Luedtke, E. Bogachek, and H. Cheng, Science, **267**(5205), 1793, 1995.

[17] U. Landman, W. Luedtke, B. Salisbury, and R. Whetten, Physical Review Letters, **77**(7), 1362–1365, 1996.

[18] Z. Gai, Y. He, H. Yu, and W. Yang, Physical Review B, **53**(3), 1042–1045, 1996.

[19] X. Zhou, Y. Wei, L. Liu, Z. Chen, J. Tang, and B. Mao, Journal of the American Chemical Society, **130**(40), 13228–13230, 2008.

[20] J. Gimzewski and C. Joachim, Science, **283**(5408), 1683, 1999.

[21] Z. Donhauser, B. Mantooth, K. Kelly, L. Bumm, J. Monnell, J. Stapleton, D. Price Jr, A. Rawlett, D. Allara, and J. Tour, Science, **292**(5525), 2303, 2001.

[22] F. Fan, J. Yang, L. Cai, D. Price Jr, S. Dirk, D. Kosynkin, Y. Yao, A. Rawlett, J. Tour, and A. Bard, J. Am. Chem. Soc, **124**(19), 5550–5560, 2002.

[23] B. Xu and N. Tao, Science, **301**(5637), 1221, 2003.

[24] Z. Huang, F. Chen, R. D'agosta, P. Bennett, M. Di Ventra, and N. Tao, Nature Nanotechnology, **2**(11), 698–703, 2007.

[25] W. Haiss, H. van Zalinge, S. Higgins, D. Bethell, H. Hobenreich, D. Schiffrin, and R. Nichols, J. Am. Chem. Soc, **125**(50), 15294–15295, 2003.

[26] W. Haiss, R. Nichols, H. Zalinge, S. Higgins, D. Bethell, and D. Schiffrin, Physical Chemistry Chemical Physics, **6**(17), 4330–4337, 2004.

[27] J. Tersoff and D. Hamann, Physical Review B, **31**(2), 805–813, 1985.

[28] V. Mujica, M. Kemp, and M. Ratner, The Journal of Chemical Physics, **101**, 6856, 1994.

[29] V. Mujica, M. Kemp, and M. Ratner, The Journal of Chemical Physics, **101**, 6849, 1994.

[30] W. Tian, S. Datta, S. Hong, R. Reifenberger, J. Henderson, and C. Kubiak, The Journal of Chemical Physics, **109**, 2874, 1998.

[31] M. Olson, Y. Mao, T. Windus, M. Kemp, M. Ratner, N. Leon, and V. Mujica, The Journal of Physical Chemistry B, **102**(6), 941–947, 1998.

[32] E. Emberly and G. Kirczenow, Physical Review B, **58**(16), 10911, 1998.

[33] M. Samanta, W. Tian, S. Datta, J. Henderson, and C. Kubiak, Physical Review B, **53**(12), 7626–7629, 1996.

[34] S. Yaliraki, M. Kemp, and M. Ratner, Journal of the American Chemical Society, **121**(14), 3428–3434, 1999.

[35] S. Yaliraki, A. Roitberg, C. Gonzalez, V. Mujica, and M. Ratner, The Journal of Chemical Physics, **111**, 6997, 1999.

[36] Y. Xue, S. Datta, and M. Ratner, The Journal of Chemical Physics, **115**, 4292, 2001.

[37] A. Ghosh, F. Zahid, S. Datta, and R. Birge, Chemical Physics, **281**(2-3), 225–230, 2002.

[38] N. Lang and P. Avouris, Physical Review B, **64**(12), 125323, 2001.

[39] M. Di Ventra, S. Pantelides, and N. Lang, Physical Review Letters, **84**(5), 979–982, 2000.

[40] J. Seminario, C. De La Cruz, and P. Derosa, JOURNAL-AMERICAN CHEMICAL SOCIETY, **123**(23), 5616–5617, 2001.

[41] K. Stokbro, J. Taylor, M. Brandbyge, and P. Ordejon, Annals of the New York Academy of Sciences, **1006**(1), 212–226, 2003.

[42] M. Brandbyge, J. L. Mozos, P. Ordejon, J. Taylor, and K. Stokbro, Physical Review B, **65**(16), 165401, 2002. PRB.

[43] J. Taylor, H. Guo, and J. Wang, Physical Review B, **63**(24), 245407, 2001. PRB.

[44] C. Wang, Y. Fu, and Y. Luo, Physical Chemistry Chemical Physics, **3**(22), 5017–5023, 2001.

[45] C. Wang and Y. Luo, The Journal of Chemical Physics, **119**, 4923, 2003.

[46] A. Troisi and M. Ratner, Small, **2**(2), 172–181, 2006.

[47] M. Galperin, M. Ratner, and A. Nitzan, Journal of Physics: Condensed Matter, **19**, 103201, 2007.

[48] R. C. Jaklevic and J. Lambe, Physical Review Letters, **17**(22), 1139, 1966.

REFERENCES

[49] B. Stipe, M. Rezaei, and W. Ho, Science, **280**(5370), 1732, 1998.

[50] K. Makoshi and N. Mingo, Surface Science, **502**, 34–40, 2002.

[51] N. Mingo and K. Makoshi, Physical Review Letters, **84**(16), 3694–3697, 2000.

[52] N. Lorente, M. Persson, L. Lauhon, and W. Ho, Physical Review Letters, **86**(12), 2593–2596, 2001.

[53] E. Emberly and G. Kirczenow, Physical Review B, **61**(8), 5740, 2000.

[54] H. Ness, S. Shevlin, and A. Fisher, Physical Review B, **63**(12), 125422, 2001.

[55] H. Ness and A. Fisher, Physical Review Letters, **83**(2), 452–455, 1999.

[56] Z. Yu, D. Smith, A. Saxena, and A. Bishop, Physical Review B, **59**(24), 16001, 1999.

[57] A. Troisi, M. A. Ratner, and A. Nitzan, Journal of Chemical Physics, **118**(13), 6072–6082, 2003.

[58] M. Paulsson, T. Frederiksen, and M. Brandbyge, Nano Letters, **6**(2), 258–262, 2006.

[59] W. Y. Wang, T. Lee, and M. A. Reed, Journal of Physical Chemistry B, **108**(48), 18398–18407, 2004.

[60] J. Jiang, M. Kula, W. Lu, and Y. Luo, Nano Letters, **5**(8), 1551–1555, 2005.

[61] M. Kula, J. Jiang, and Y. Luo, Nano Letters, **6**(8), 1693–1698, 2006.

[62] J. Jiang, M. Kula, and Y. Luo, Journal of Physics-Condensed Matter, **20**(37), 374110(12), 2008.

[63] M. Kula and Y. Luo, Journal of Chemical Physics, **128**(6), 064705(7), 2008.

[64] E. Petrov and V. May, The Journal of Physical Chemistry A, **105**(45), 10176–10186, 2001.

[65] E. Petrov, V. May, and P. Hanggi, Chemical Physics, **281**(2-3), 211–224, 2002.

[66] Y. Berlin, A. Burin, and M. Ratner, Journal of the American Chemical Society, **123**(2), 260, 2001.

[67] M. Bixon, B. Giese, S. Wessely, T. Langenbacher, M. Michel-Beyerle, and J. Jortner, Proceedings of the National Academy of Sciences, **96**(21), 11713, 1999.

[68] E. Schlag, D. Yang, S. Sheu, H. Selzle, S. Lin, and P. Rentzepis, Proceedings of the National Academy of Sciences, **97**(18), 9849, 2000.

[69] Q. Lu, K. Liu, H. Zhang, Z. Du, X. Wang, and F. Wang, Acs Nano, **3**(12), 3861–3868, 2009.

[70] D. Visontai, I. Grace, and C. Lambert, Physical Review B, **81**(3), 35409, 2010.

[71] T. Hines, I. Diez-Perez, J. Hihath, H. Liu, Z. Wang, J. Zhao, G. Zhou, K. Mu llen, and N. Tao, Journal of the American Chemical Society, **132**(33), 11658–11664, 2010.

[72] S. Choi, C. Risko, M. Delgado, B. Kim, J. Bredas, and C. Frisbie, Journal of the American Chemical Society, **132**(12), 4358–4368, 2010.

[73] A. Nitzan, Annual Review of Physical Chemistry, **52**(1), 681–750, 2001.

[74] A. Nitzan and M. Ratner, Science, **300**(5624), 1384, 2003.

[75] G. Nan, X. Yang, L. Wang, Z. Shuai, and Y. Zhao, Physical Review B, **79**(11), 115203, 2009.

[76] Y. Liu, X. Fan, D. Yang, C. Wang, L. Wan, and C. Bai, Chemical Physics Letters, **380**(5-6), 767–773, 2003.

[77] F. Chen, Z. Huang, and N. Tao, Applied Physics Letters, **91**(16), 162106, 2009.

[78] C. Ko, M. Huang, M. Fu, and C. Chen, Journal of the American Chemical Society, **132**(2), 756–764, 2009.

[79] H. Kondo, J. Nara, H. Kino, and T. Ohno, Journal of Physics: Condensed Matter, **21**, 064220, 2009.

[80] L. Venkataraman, J. Klare, C. Nuckolls, M. Hybertsen, and M. Steigerwald, Nature, **442**(7105), 904–907, 2006.

[81] C. George, M. Ratner, and J. Lambert, The Journal of Physical Chemistry A, **113**(16), 3876–3880, 2009.

[82] C. Silva Jr, S. da Silva, E. Granhen, J. Leal, J. Del Nero, and F. Pinheiro, PHYSICAL REVIEW B Phys Rev B, **82**, 085402, 2010.

[83] L. Venkataraman, Y. Park, A. Whalley, C. Nuckolls, M. Hybertsen, and M. Steigerwald, Nano Letters, **7**(2), 502–506, 2007.

[84] J. Quinn, F. Foss Jr, L. Venkataraman, and R. Breslow, J. Am. Chem. Soc, **129**(41), 12376–12377, 2007.

[85] E. Leary, S. Higgins, H. Zalinge, W. Haiss, and R. Nichols, Chemical Communications, **2007**(38), 3939–3941, 2007.

REFERENCES

[86] J. Palma, C. Cao, X. Zhang, P. Krstic, J. Krause, and H. Cheng, The Journal of Physical Chemistry C, **114**(3), 1655–1662, 2010.

[87] P. Priya, C. Kala, and D. Thiruvadigal, Int. J. Nanoelectronics and Materials, **3**, 1–7, 2010.

[88] M. Strange, O. Lopez-Acevedo, and H. Ha kkinen, The Journal of Physical Chemistry Letters, **1**(10), 1528–1532, 2010.

[89] Y. Jang and W. Goddard III, The Journal of Physical Chemistry C, **114**(10), 4646–4651, 2010.

[90] D. Luzhbin and C. Kaun, Physical Review B, **81**(3), 35424, 2010.

[91] F. Chen, X. Li, J. Hihath, Z. Huang, and N. Tao, J. Am. Chem. Soc, **128**(49), 15874–15881, 2006.

[92] S. Martin, W. Haiss, S. Higgins, P. Cea, M. Lopez, and R. Nichols, The Journal of Physical Chemistry C, **112**(10), 3941–3948, 2008.

[93] Z. Li and D. Kosov, J. Phys. Chem. B, **110**(20), 9893–9898, 2006.

[94] C. Martin, D. Ding, J. Sorensen, T. Bjornholm, J. van Ruitenbeek, and H. van der Zant, J. Am. Chem. Soc, **130**(40), 13198–13199, 2008.

[95] C. Li, I. Pobelov, T. Wandlowski, A. Bagrets, A. Arnold, and F. Evers, J. Am. Chem. Soc, **130**(1), 318–326, 2008.

[96] A. Nishikawa, J. Tobita, Y. Kato, S. Fujii, M. Suzuki, and M. Fujihira, Nanotechnology, **18**, 424005, 2007.

[97] X. Li, J. He, J. Hihath, B. Xu, S. Lindsay, and N. Tao, J. Am. Chem. Soc, **128**(6), 2135–2141, 2006.

[98] N. Weibel, A. B aszczyk, C. von Hanisch, M. Mayor, I. Pobelov, T. Wandlowski, F. Chen, and N. Tao, European Journal of Organic Chemistry, **2008**(1), 136–149, 2008.

[99] A. Yanson and R. Bollinger, Nature, **395**(6704), 783–785, 1998.

[100] X. Xiao, B. Xu, and N. Tao, Nano Letters, **4**(2), 267–271, 2004.

[101] L. Venkataraman, J. Klare, I. Tam, C. Nuckolls, M. Hybertsen, and M. Steigerwald, Nano Letters, **6**(3), 458–462, 2006.

[102] J. Ulrich, D. Esrail, W. Pontius, L. Venkataraman, D. Millar, and L. Doerrer, J. Phys. Chem. B, **110**(6), 2462–2466, 2006.

[103] X. Li, J. Hihath, F. Chen, T. Masuda, L. Zang, and N. Tao, J. Am. Chem. Soc, **129**(37), 11535–11542, 2007.

[104] D. Jones and A. Troisi, The Journal of Physical Chemistry C, **111**(39), 14567–14573, 2007.

[105] W. Wang, T. Lee, and M. Reed, Physical Review B, **68**(3), 35416, 2003.

[106] W. Haiss, H. Zalinge, D. Bethell, J. Ulstrup, D. Schiffrin, and R. Nichols, Faraday Discussions, **131**, 253–264, 2006.

[107] S. Marti n, F. Giustiniano, W. Haiss, S. Higgins, R. Whitby, and R. Nichols, The Journal of Physical Chemistry C, **113**(43), 18884–18890, 2009.

[108] H. Akkerman, A. Kronemeijer, J. Harkema, P. van Hal, E. Smits, D. de Leeuw, and P. Blom, Organic Electronics, **11**(1), 146–149, 2010.

[109] A. Salomon, H. Shpaisman, O. Seitz, T. Boecking, and D. Cahen, J. Phys. Chem, **100**(112), 3969–3974, 2008.

[110] Y. Selzer, M. Cabassi, T. Mayer, and D. Allara, J. Am. Chem. Soc, **126**(13), 4052–4053, 2004.

[111] H. Cao, J. Jiang, J. Ma, and Y. Luo, Journal of the American Chemical Society, **130**(21), 6674–6675, 2008.

[112] D. Wold and C. Frisbie, Journal of the American Chemical Society, **123**(23), 5549–5556, 2001.

[113] T. Ishida, W. Mizutani, Y. Aya, H. Ogiso, S. Sasaki, and H. Tokumoto, The Journal of Physical Chemistry B, **106**(23), 5886–5892, 2002.

[114] E. Emberly and G. Kirczenow, Physical Review B, **64**(23), 235412, 2001.

[115] R. Liu, S. Ke, H. Baranger, and W. Yang, The Journal of Chemical Physics, **122**, 044703, 2005.

[116] H. Geng, S. Yin, K. Chen, and Z. Shuai, J. Phys. Chem. B, **109**(25), 12304–12308, 2005.

[117] H. Geng, Y. Hu, Z. Shuai, K. Xia, H. Gao, and K. Chen, The Journal of Physical Chemistry C, **111**(51), 19098–19102, 2007.

[118] M. Long, K. Chen, L. Wang, B. Zou, and Z. Shuai, Applied Physics Letters, **91**, 233512, 2007.

[119] T. Dittrich, P. Hanggi, G. Schon, and B. Kramer. *Quantum transport and dissipation*. Wiley-VCH, 1998.

REFERENCES

[120] J. R. Tayor. *Scattering Theory*. Wiley, New York, 1972.

[121] J. Jiang and Y. Luo, Royal Institute of Technology, **Sweden**, thanks to Chuan–Kui Wang and Ying Fu, Stockholm.

[122] J. Jiang, Royal Institute of Technology, **Sweden**, Stockholm.

[123] M. Frisch, G. Trucks, H. Schlegel, G. Scuseria, M. Robb, J. Cheeseman, G. Scalmani, V. Barone, B. Mennucci, and G. Petersson, Inc.: Wallingford, CT, 2009.

[124] J. Jiang, W. Lu, and Y. Luo, Chemical Physics Letters, **400**(4-6), 336–340, 2004.

[125] A. Rocha, V. Garcia-Suarz, S. Bailey, C. Lambert, J. Ferrer, and S. Sanvito, Nature Materials, **4**(4), 335–339, 2005.

[126] A. Rocha, V. Garcia-Suarez, S. Bailey, C. Lambert, J. Ferrer, and S. Sanvito, Physical Review B, **73**(8), 085414, 2006.

[127] S. Yaliraki and M. Ratner, The Journal of Chemical Physics, **109**, 5036, 1998.

[128] N. Lang and P. Avouris, Physical Review B, **62**(11), 7325, 2000.

[129] S. Wu, M. Gonzolez, R. Huber, S. Grunder, M. Mayor, C. Schonenberger, and M. Calame, Nature Nanotechnology, **3**(9), 569–574, 2008.

[130] M. Reed, Materials Today, **11**(11), 46–50, 2008.

[131] L. Lin, C. Wang, and Y. Luo, Acs Nano, 2011.

[132] J. Jiang, M. Kula, and Y. Luo, The Journal of Chemical Physics, **124**, 034708, 2006.

[133] J. Klein, A. Leger, M. Belin, D. Defourneau, and M. Sangster, Physical Review B, **7**(6), 2336, 1973.

[134] A. Troisi and M. Ratner, Phys. Chem. Chem. Phys., **9**(19), 2421–2427, 2007.

[135] J. Kirtley, D. Scalapino, and P. Hansma, Physical Review B, **14**(8), 3177, 1976.

[136] A. Troisi and M. Ratner, Nano Letters, **6**(8), 1784–1788, 2006.

[137] M. Paulsson, T. Frederiksen, H. Ueba, N. Lorente, and M. Brandbyge, Physical Review Letters, **100**(22), 2008.

[138] A. Troisi, Chem. Soc. Rev., 2011.

[139] J. Chang, T. Sakanoue, Y. Olivier, T. Uemura, M. Dufourg-Madec, S. Yeates, J. Cornil, J. Takeya, A. Troisi, and H. Sirringhaus, Physical Review Letters, **107**(6), 66601, 2011.

[140] M. Yamagishi, J. Soeda, T. Uemura, Y. Okada, Y. Takatsuki, T. Nishikawa, Y. Nakazawa, I. Doi, K. Takimiya, and J. Takeya, Physical Review B, **81**(16), 161306, 2010.

[141] T. Holstein, Annals of Physics, **8**(3), 325–342, 1959.

[142] T. Holstein, Annals of Physics, **8**(3), 343–389, 1959.

[143] R. Silbey and R. Munn, The Journal of Chemical Physics, **72**, 2763, 1980.

[144] R. Munn and R. Silbey, The Journal of Chemical Physics, **83**, 1854, 1985.

[145] K. Hannewald and P. Bobbert, Applied Physics Letters, **85**, 1535, 2004.

[146] K. Hannewald, V. Stojanovic, and P. Bobbert, Journal of Physics: Condensed Matter, **16**, 2023, 2004.

[147] K. Hannewald, V. Stojanovic, J. Schellekens, P. Bobbert, G. Kresse, and J. Hafner, Physical Review B, **69**(7), 075211, 2004.

[148] J. Jortner, The Journal of Chemical Physics, **64**, 4860, 1976.

[149] S. H. Lin, C. H. Chang, K. K. Liang, R. Chang, Y. J. Shiu, J. M. Zhang, T. S. Yang, M. Hayashi, and F. C. Hsu. Ultrafast dynamics and spectroscopy of bacterial photosynthetic reaction centers. pages 1–88. 2002.

[150] A. Troisi and G. Orlandi, The Journal of Physical Chemistry B, **106**(8), 2093–2101, 2002.

[151] X. Yang, L. Wang, C. Wang, W. Long, and Z. Shuai, Chemistry of Materials, **20**(9), 3205–3211, 2008.

[152] E. Valeev, V. Coropceanu, D. da Silva Filho, S. Salman, and J. Bredas, Journal of the American Chemical Society, **128**(30), 9882–9886, 2006.

[153] M. Winkler and K. Houk, Journal of the American Chemical Society, **129**(6), 1805–1815, 2007.

[154] C. Wang, B. Zou, X. Song, Y. Li, Z. Li, and L. Lin, Frontiers of Physics in China, **4**(3), 415–419, 2009.

[155] J. Reimers, Journal of Chemical Physics, **115**(20), 9103–9109, 2001.

[156] W. Pasveer, J. Cottaar, C. Tanase, R. Coehoorn, P. Bobbert, P. Blom, D. De Leeuw, and M. Michels, Physical Review Letters, **94**(20), 206601, 2005.

[157] J. Kirkpatrick, V. Marcon, K. Kremer, J. Nelson, and D. Andrienko, The Journal of Chemical Physics, **129**, 094506, 2008.

[158] H. Song, Y. Kim, Y. Jang, H. Jeong, M. Reed, and T. Lee, Nature, **462**(7276), 1039–1043, 2009.

[159] M. Taniguchi, M. Tsutsui, K. Yokota, and T. Kawai, Nanotechnology, **20**, 434008, 2009.

[160] M. Tsutsui, M. Taniguchi, K. Shoji, K. Yokota, and T. Kawai, Nanoscale, **1**(1), 164–170, 2009.

[161] H. Song, Y. Kim, J. Ku, Y. Jang, H. Jeong, and T. Lee, Applied Physics Letters, **94**, 103110, 2009.

[162] A. Troisi and M. Ratner, Physical Review B, **72**(3), 33408, 2005.

[163] J. Beebe, H. Moore, T. Lee, and J. Kushmerick, Nano Letters, **7**(5), 1364–1368, 2007.

[164] N. Okabayashi, M. Paulsson, H. Ueba, Y. Konda, and T. Komeda, Nano Letters, **10**(8), 2950, 2010.

[165] J. Hihath, C. Arroyo, G. Rubio-Bollinger, N. Tao, and N. Agrait, Nano Letters, **8**(6), 1673–1678, 2008.

[166] B. Jones, M. Ahrens, M. Yoon, A. Facchetti, T. Marks, and M. Wasielewski, Angewandte Chemie, **116**(46), 6523–6526, 2004.

[167] A. Molinari, H. Alves, Z. Chen, A. Facchetti, and A. Morpurgo, Journal of the American Chemical Society, **131**(7), 2462–2463, 2009.

[168] N. Minder, S. Ono, Z. Chen, A. Facchetti, and A. Morpurgo, Advanced Materials, **24**(4), 503–508, 2012.